Oligomerization and endocytosis of Hedgehog is necessary for its efficient exovesicular secretion

Anup Parchure[a], Neha Vyas[b], Charles Ferguson[c], Robert G. Parton[c], and Satyajit Mayor[a,b]
[a]National Centre for Biological Sciences and [b]Institute for Stem Cell Biology and Regenerative Medicine, Tata Institute of Fundamental Research, Bangalore 560065, India; [c]Institute for Molecular Bioscience and Centre for Microscopy and Microanalysis, University of Queensland, Brisbane St Lucia 4072, Australia

ABSTRACT **Hedgehog (Hh) is a secreted morphogen involved in both short- and long-range signaling necessary for tissue patterning during development. It is unclear how this dually lipidated protein is transported over a long range in the aqueous milieu of interstitial spaces. We previously showed that the long-range signaling of Hh requires its oligomerization. Here we show that Hh is secreted in the form of exovesicles. These are derived by the endocytic delivery of cell surface Hh to multivesicular bodies (MVBs) via an endosomal sorting complex required for transport (ECSRT)–dependent process. Perturbations of ESCRT proteins have a selective effect on long-range Hh signaling in *Drosophila* wing imaginal discs. Of importance, oligomerization-defective Hh is inefficiently incorporated into exovesicles due to its poor endocytic delivery to MVBs. These results provide evidence that nanoscale organization of Hh regulates the secretion of Hh on ESCRT-derived exovesicles, which in turn act as a vehicle for long-range signaling.**

Monitoring Editor
Benjamin S. Glick
University of Chicago

Received: Sep 23, 2015
Accepted: Oct 14, 2015

INTRODUCTION

Secreted morphogens are signaling molecules produced from a source and lead to the activation of different target genes in a distal set of cells capable of receiving these signals. The resulting graded response generates distinct tissue types in the morphogenetic field. Distinct cellular processes operate in generating and receiving this signal, resulting in a well-defined and reproducible tissue pattern (Tabata and Takei, 2004).

Hedgehog (Hh) is one of the prime examples of such secreted morphogens. Originally discovered in *Drosophila* (Nüsslein-Volhard and Wieschaus, 1980), Hh signaling is important in embryonic patterning, larval development, and in maintenance of tissue architecture and repair in adults (Michel *et al.*, 2012). The loss of Hh results in several developmental defects, including cyclopia (Chiang *et al.*, 1996). Hh signal is transduced via the primary cilium in the receiving cells (Nozawa *et al.*, 2013). Binding of Hh to its receptor Patched (Ptc) relieves Smoothened (Smo) repression, leading to phosphorylation of Smo, Fused, and Cos2. This in turn leads to translocation to active Cubitus interruptus (Ci) to the nucleus for target-gene activation (Briscoe and Thérond, 2013).

Many of these primary insights regarding the role of Hh have come from studying the function of Hh in *Drosophila*. Its role as a long-range morphogen has been best studied in the *Drosophila* wing imaginal disc (Torroja *et al.*, 2005) and also in the development of the vertebrate neural tube (Dessaud *et al.*, 2008). In the *Drosophila* wing imaginal disc, although Hh is produced by the cells in the posterior compartment, it acts on cells in the anterior compartment, where its receptor, Ptc, is expressed, several cell diameters away from the source cells. This signaling eventually leads to the patterning of the L3–L4 intervein distance, as well as formation of wing bristles (Torroja *et al.*, 2005) in adult flies. Many molecular players in the Hh pathway have been discovered using this feature as readout for Hh function (Burke *et al.*, 1999; Katanaev *et al.*, 2008; Aikin *et al.*, 2012).

Hh, synthesized as a 45-kDa precursor protein (Porter *et al.*, 1995), undergoes an autocatalytic replacement of the C-terminal domain with a cholesterol moiety and is further modified by palmitoylation at its N-terminus (Porter *et al.*, 1995; Pepinsky *et al.*, 1998). These modifications are responsible for its tight association with

This article was published online ahead of print in MBoC in Press (http://www.molbiolcell.org/cgi/doi/10.1091/mbc.E15-09-0671) on October 21, 2015.

Address correspondence to: Satyajit Mayor (mayor@ncbs.res.in).

Abbreviations used: A647–anti-GFP Fab, Alexa 647–labeled anti–GFP Fab; EM, electron microscopy; ESCRT, endosomal sorting complex required for transport; FCS, fluorescence correlation spectroscopy; GFP, green fluorescent protein; Hh, Hedgehog; HSPG, heparan sulfate proteoglycans; ILV, intraluminal vesicle; mCFP, monomeric cyan fluorescent protein; MVB, multivesicular body; RNAi, RNA interference; TMR-Dex, tetramethyl rhodamine–conjugated dextran.

membranes (Peters *et al.*, 2004; Tukachinsky *et al.*, 2012). It is therefore surprising that despite being membrane anchored, Hh activates paracrine long-range signaling.

Different mechanisms have been proposed to explain the transport of Hh over a long range. Hh has been shown to associate with lipoprotein particles, which are made in the fat body and thereby circulate in the hemolymph, effecting long-range Hh signaling (Panáková *et al.*, 2005). At the apical and basolateral faces of the epithelium in wing imaginal discs, Hh has been suggested to spread by two distinct mechanisms. At the apical surface, its association with the glycipan Dally and the activity of hydrolase Notum has been postulated in effecting its long- range transport (Ayers *et al.*, 2010). In the basal surface of both wing imaginal disc and abdominal epidermis, dynamic activity of cytoskeletal extensions called the cytonemes appears to dictate formation of the Hh gradient (Bischoff *et al.*, 2013).

However, the form(s) of Hh recruited to these transport pathways remain unclear. It has been proposed that Hh will associate with the lipoprotein particle by virtue of its hydrophobic attachments. Punctate structures of Hh have been visualized in the basal epithelium of the wing imaginal disc along the cytonemes (Bischoff *et al.*, 2013). In *Caenorhabditis elegans*, V0-ATPase mediates apical secretion of Hh-related peptides containing exosomes (Liégeois *et al.*, 2006). Another lipid-tethered morphogen, Wingless (Wg), is released on exosome-like vesicles in cell culture–based assays (Gross *et al.*, 2012; Beckett *et al.*, 2013), which play an important role in Wg signaling (Gross *et al.*, 2012). Recent work suggests that Hh is secreted in the form of exosome-like vesicles, and these are transported by cytonemes to effect long-range Hh signaling in the wing imaginal disc (Gradilla *et al.*, 2014). In a separate study, the generation of exovesicles was proposed to occur via surface blebbing pathways (Matusek *et al.*, 2014).

In earlier work from our laboratory, we showed that long-range signaling by Hh required its homo-oligomerization (Vyas *et al.*, 2008). Contrary to the proposed mechanism (Matusek *et al.*, 2014), we provide evidence that exovesicular secretion of Hh occurs via a multivesicular body (MVB)–dependent mechanism that uses the core endosomal sorting complexes required for transport (ESCRT) proteins Vps28 and Shrub and the regulatory proteins Vps4 and Alix. Our results also show that Hh organization is necessary for its secretion. We find that Hh is secreted in multiple exovesicular forms differing in both biochemical and physical properties. Hh traffics from the cell surface to the MVBs, and by perturbations in genes involved in endocytosis, MVB biogenesis, and fusion, we show that generation of exovesicular carriers requires endocytic delivery of Hh from the cell surface into MVBs and packaging into intraluminal vesicles (ILVs). We reasoned that oligomerization could be important for incorporation of Hh into these carriers. Indeed, oligomerization-defective Hh has a defect in exovesicular secretion, primarily due to reduced endocytosis required for delivery to MVBs, consistent with our hypothesis. Perturbations in ESCRT proteins trap Hh in enlarged endocytic compartments, which affect its secretion and long-range signaling in the wing imaginal disc, proving a crucial role for released exoveiscles in long-range transport of Hh.

RESULTS

Characterization of secreted forms of Hh

To characterize the nature of the secreted form of Hh, we expressed it in insect cells and analyzed the biochemical and biophysical properties of Hh released into the culture medium. We used differential centrifugation–based fractionation (Figure 1A) of the culture medium derived from S2R+ cell lines transfected with native Hh. Hh was detected in three distinct fractions (Figure 1B): two corresponding to the 100,000 × *g* and 250,000 × *g* pellets, P100 and P250, respectively; and a third corresponding to the 250,000 × *g* supernatant, S250.

To characterize these forms further, we expressed green fluorescent protein (GFP)–tagged Hh (HhGFP) in S2R+ cells. Previously we showed the rescue of the temperature-sensitive Hh^{ts2} mutant grown at the restrictive temperature by this fusion construct (Vyas *et al.*, 2008). As observed for the untagged form, HhGFP was also secreted in three different fractions by S2R+ cells (Figure 1B). On resuspension, the P100 fraction contained two species diffusing at times scales separated by a factor of seven to eight from each other as measured with fluorescence correlation spectroscopy (FCS; Figure 1, C and D, and Table 1).

The sizes of these forms could be estimated by comparing their diffusion coefficients with that of GFP, a protein with a 2.8-nm hydrodynamic radius (D = 83.7 ± 3.7 $\mu m^2/s$). This comparison suggested that the size of the slow-diffusing species present in the P100 corresponded to that of typical exosomes (~60–80 nm), whereas the fast-diffusing species was smaller (~12–14 nm). FCS measurements on P250 provided evidence for a single fast-diffusing species similar to the fast-diffusing species in the P100 form, suggesting that it was composed of only the ~12- to 14-nm form. Because the diffusion coefficient of the form present in the S250 fraction was similar to GFP in solution, we did not look for any further pelleting forms from this supernatant (Figure 1, C and D, and Table 1).

Hh is known to be associated with lipoprotein particles (Panáková *et al.*, 2005). In culture conditions, serum is the source of lipoproteins for growing cells. Hence we cultured cells in serum-incomplete medium lacking lipoproteins. We continued to observe the presence of HhGFP in P100 and P250 fractions, but it was absent from the S250 fraction (Figure 1B). Because depletion of serum can also result in removal of important growth factors, we grew cells in medium depleted of serum vesicles by pelleting fresh medium at 250,000 × *g*. HhGFP continued to be secreted in all three fractions (Supplemental Figure S1B). This suggested that both P100 and P250 fractions contain bona fide secretory forms of cellular origin, whereas the Hh that is present in the S250 fraction is a likely product of serum-derived protease activity.

We next used immuno-electron microscopy (EM) followed by negative staining for morphological characterization of the material isolated in the P100 and P250 fractions. Vesicle-like structures were visualized when labeled with an anti-Hh antibody in both fractions (Figure 1E and Supplemental Figure S2, A and B). The vesicles in the P100 fraction showed a broad size distribution (ranging from 20 to 110 nm), whereas the vesicles in the P250 fraction were of uniform size, centered around 20–40 nm (Figure 1F), in good agreement with the smaller size in FCS measurements. Whereas the smaller vesicles in the P250 fraction have mainly one gold particle on them, we observed vesicles with more than one gold particle in the P100 fraction (Supplemental Figure S2D).

We further determined the topology of GFP on these vesicles by using a protease protection assay and found that all of the protein was degraded in the presence as well as absence of detergent (Supplemental Figure S1C), indicating that Hh must face the exterior of these vesicles. Of importance, P100 and P250 fractions containing HhGFP could activate an Hh signaling response determined using a luciferase signaling assay in Clone8 cells (Yan *et al.*, 2010; Figure 1G). The level of signaling we obtain is related to the limitation of obtaining significant amounts of Hh in pelleted fractions, as increasing this amount using a highly secreted cholesterol-deficient (HhN) variant of Hh results in more signaling (unpublished data). Taken together, these properties suggest that the secreted forms of

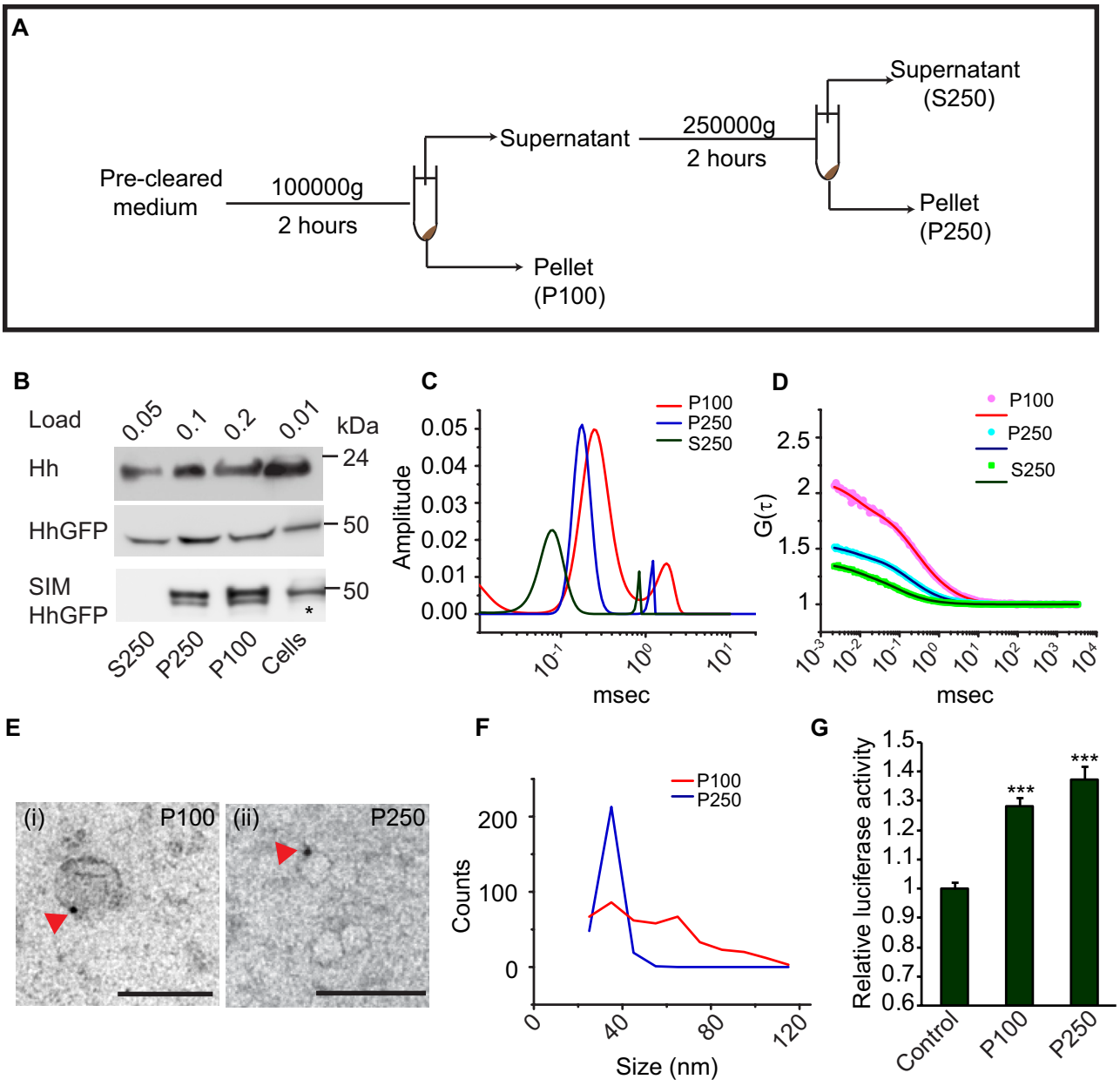

FIGURE 1: Hh is secreted by insect cells as exovesicles. (A) Experimental strategy for the isolation of exovesicles. (B) Western blots of the indicated fractions probed with anti-Hh (top) or anti-GFP (middle and bottom) antibodies show the presence of secreted Hh or HhGFP in the 100,000 × *g* (P100) and the 250,000 × *g* (P250) pellets, as well as in the supernatant (S250). The bands were visualized by loading the indicated amount of material for each fraction, derived from insect cells expressing actin-Gal4 and UAS-Hh or UAS-HhGFP (top). Asterisk indicates half the amount of sample loaded for cellular fraction only. Note that cells grown in serum-free medium (SIM) show an absence of the Hh band in the S250 fraction. (C, D) Distributions of diffusion time scales (C) of the different species present in the indicated fractions derived from the autocorrelation analysis of FCS data (D, dotted lines) obtained from analyzing fluorescence fluctuations in a confocal microscope of fractions P100 (red line), P250 (blue line), and S250 (green line). The distribution of time scales were obtained using the maximum entropy method (MEM) fitting routine and was used to compute the two-component, 3D diffusion fit of the FCS traces (solid lines in D). (E) Immuno-EMs show the most frequent exovesicle-like structures in the P100 (i) and P250 (ii) fractions, labeled using anti-Hh antibody and probed using 5-nm protein A–gold (arrowheads). Scale bar, 100 nm. (F) A broad size distribution of vesicle sizes is observed in the P100 (red line) fraction compared with P250 (blue line). The frequency distribution was obtained from the analysis of 442 vesicles in P100 and 282 vesicles in the P250 fraction. (G) Luciferase signaling assay in Clone8 cells carrying Ptc-luciferase as a reporter construct show a signaling response upon addition of HhGFP-containing P100 and P250 fractions in comparison with medium from cells that do not express HhGFP; ***$p < 0.001$.

Sample	D_1 (μm²/s)	Fraction (%)	D_2 (μm²/s)	Fraction (%)
HhGFP P100	40.1 (± 3.78)	79.5 (± 4.9)	5.40 (± 1.40)	20.4 (± 4.9)
HhGFP P250	40.8 (± 2.93)	94.9 (± 3.5)	5.66 (± 1.74)	5.1 (± 3.5)
HhGFP S250	85.5 (± 15.2)	97.3 (± 3.1)	5.52 (± 3.81)	2.7 (± 3.1)
GFP solution	83.7 (± 3.77)	5.1 (± 2.8)		

Diffusion coefficients and fractions of individual components obtained after fitting the FCS data to a two- component, 3D diffusion fit. Although the diffusion coefficients of two forms are similar in both fractions, there is a significant reduction in the fraction of the slow-diffusing component in P250 for both HhGFPs. The diffusion coefficient of the S250 form matches that of GFP in solution (last row), indicating the presence of either a monomeric or a dimeric species in the S250 form.

TABLE 1: FCS measurements of secreted fractions of HhGFP.

Hh that are biologically active are mainly associated with vesicles and have a topology and size consistent with exosomes.

Proteins of the ESCRT complex cofractionate with the vesicular forms of Hh

To characterize the biochemical properties of the vesicular forms of secreted HhGFP, we assayed for the presence of exosomal markers in the P100 and P250 fractions. As a control, we observed that GM130, a protein resident in the Golgi (Nakamura *et al.*, 1995), was absent in both of the secreted fractions (Figure 2A). Whereas proteins involved in exosomal release, such as Alix, Syntaxin 1a (Stx1a) (Matsuo *et al.*, 2004; Koles *et al.*, 2012), and the tetraspannin Late bloomer (Lbm) were present only in the P100 fraction, two proteins of the ESCRT complex—Hrs and Vps28—and the Cysteine String Protein (Csp) were found in both fractions (Figure 2A). Recent studies identified these proteins on exosome-like vesicles secreted by insect (S2) cells (Koles *et al.*, 2012; Beckett *et al.*, 2013). Sucrose gradient centrifugation has been used as an assay for exosomes (Stoeck *et al.*, 2006; Gross *et al.*, 2012; Li *et al.*, 2013). Therefore we layered both fractions on top of a sucrose gradient and assessed the densities to which HhGFP in P100 and P250 fractions sediment. Our results suggested that HhGFP sediments at densities similar (1.08–1.15) to those observed for exosomes obtained from different cell types (Meckes and Raab-Traub, 2011; Gross *et al.*, 2012; Li *et al.*, 2013). These fractions also overlapped with ESCRT proteins Hrs and Vps28 in both the fractions, consistent with their association

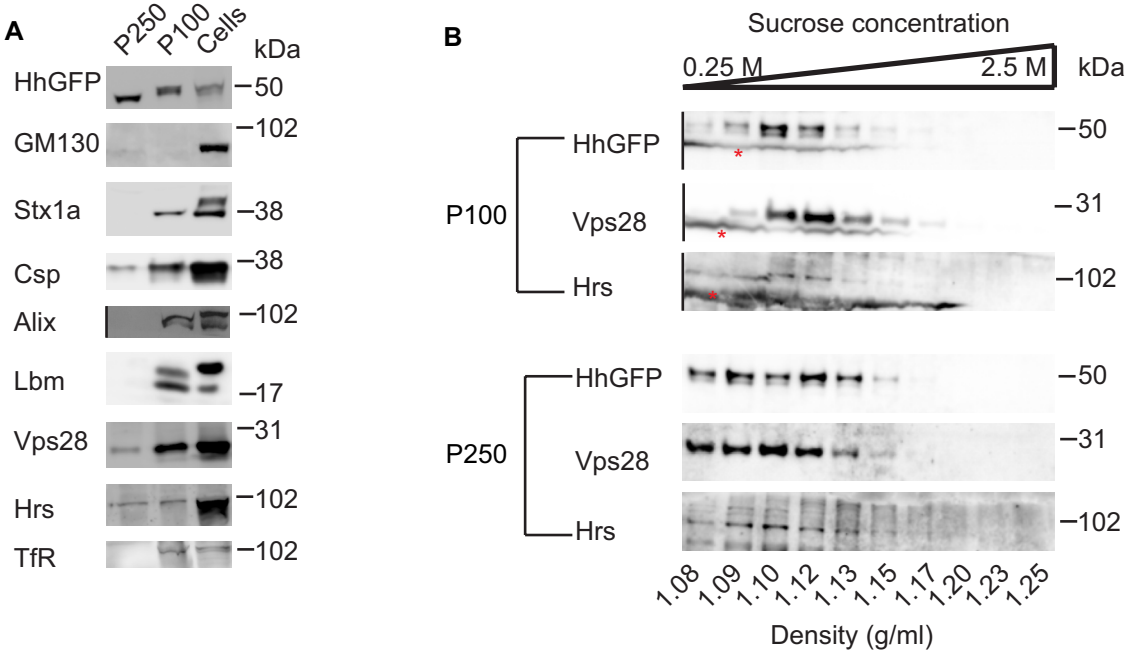

FIGURE 2: Proteins of the ESCRT complex cofractionate with secreted forms of Hh. (A) Western blots probing the presence of the indicated proteins: GM130 (Golgi matrix protein); Syntaxin 1a, Stx1a; Cysteine String Protein, Csp; ESCRT regulator, Alix; Late bloomer, Lbm; ESCRT0 protein, Hrs; ESCRT1 component, Vps28. TfR in the P100 and the P250 fractions was obtained from HhGFP-transfected S2R+ cells as described in Figure 1A. Note that whereas GM130 is absent in both fractions, exosomal markers such as Stx1a, Lbm, and Alix are observed only in P100, and Csp and the ESCRT components Hrs and Vps28 are present in both fractions. For consistent representation of images, the lane where S250 (which lacks detectable Alix protein) was loaded has been deleted, as indicated using a black vertical line in the blot for Alix. (B) Sucrose gradient sedimentation of P100 (top) and P250 (bottom) shows that HhGFP-containing vesicles migrate to densities (1.08–1.15 g/ml) that also coincide with the ESCRT components Hrs and Vps28. Asterisk indicates a nonspecific stain that occurs only in the P100 fractions and is missing from the P250 fractions. Lanes containing cell lysates from the same experiment and a marker lane have been deleted from the parent blot for representation purposes as indicated by the black vertical lines.

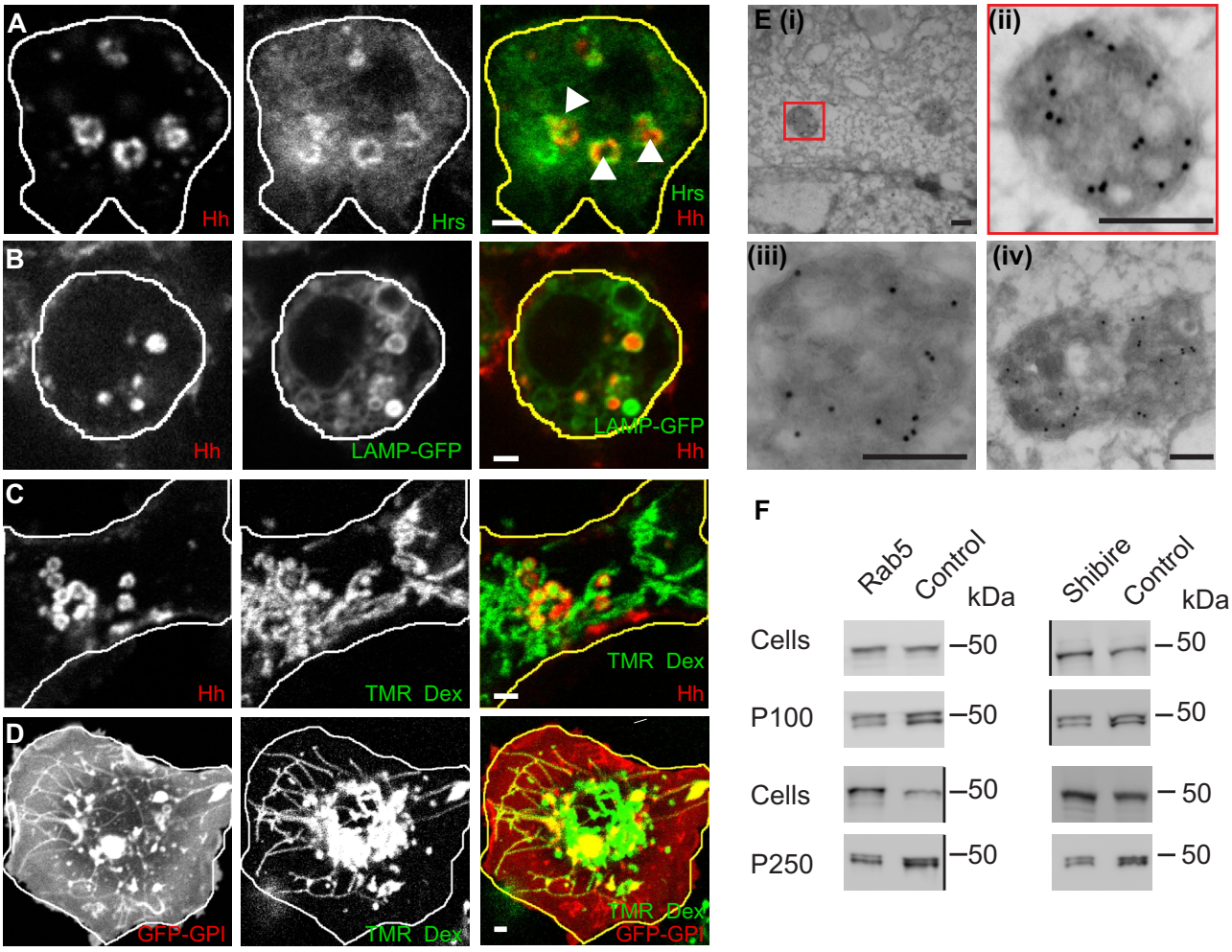

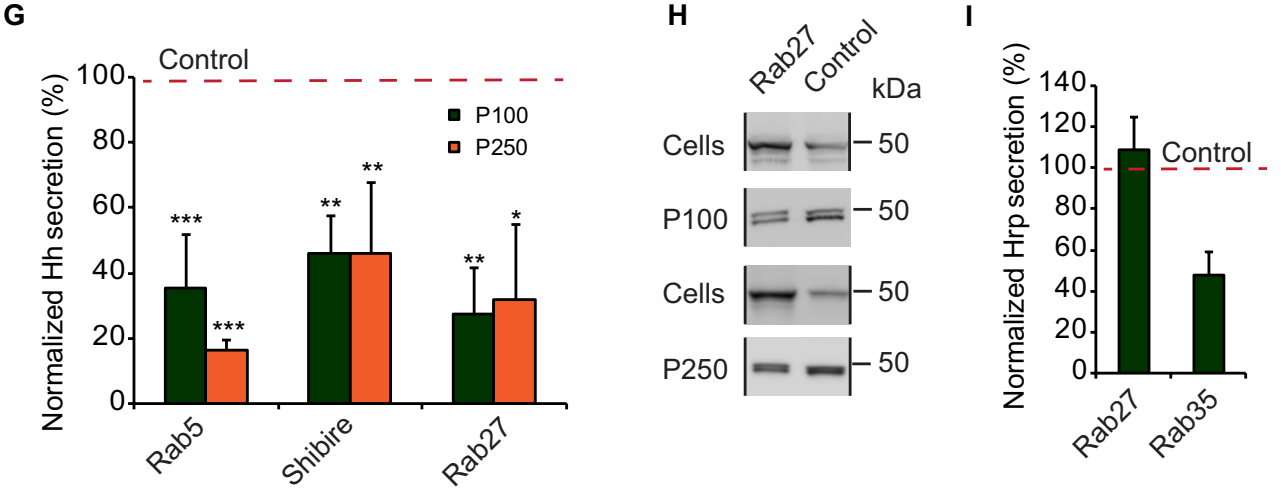

FIGURE 3: Accumulation of Hh on ILVs inside MVBs is necessary for its exovesicular secretion. (A) HhGFP-transfected S2R+ cells labeled with an endocytic pulse (2 h) of A647–anti-GFP Fab (left; red in merge) to localize endocytosed Hh and immunostained with anti-Hrs (middle; green in merge). A single confocal slice (for a 3D projection, see Supplemental Video S1). Note that A647–anti-GFP Fab staining is detected in enlarged endosomal organelles decorated with Hrs (arrowheads). Scale bar, 2 μm. (B, C) S2R+ cells were cotransfected with HhmCFP and LAMP-GFP (B) or with HhmCFP alone (C) and 2 d later incubated with A647–anti-GFP Fab singly for 20 min (B) or along with TMR-Dex for 2 h to localize organelles accessed by endocytic probes and imaged using a PerkinElmer spinning-disk confocal microscope (B) or an Olympus FV1000 confocal microscope (C). Images represent a single confocal slice (for a 3D projection of the cells, see Supplemental Video S2). Note that endocytosed Hh (left; red in merge) colocalizes with vesicular LAMP-GFP (B; middle; green in merge) and with TMR-Dex (C; middle; green in merge) only in vesicular compartments but is segregated from tubular structures representing lysosomes marked by tubular

with exovesicles (Figure 2B). We thus conclude that Hh is secreted by the S2R+ insect cells on exovesicles that cofractionate with proteins of the ESCRT machinery, are of distinct sizes, and potentially differ in their biochemical composition based on segregation of some of the known exosomal markers.

Accumulation of Hh on ILVs inside MVBs is necessary for its exovesicular secretion

The ESCRT machinery has been implicated in generating ILVs inside the MVBs (Vaccari *et al.*, 2009; Henne *et al.*, 2013). The ILVs are candidates for giving rise to exovesicles if the MVBs fuse with the cell surface. We found that not only did Hh-containing endosomes colocalize with endogenous Hrs (ESCRT0) in HhGFP-transfected cells, but there was also a redistribution of endogenous Hrs to intracellular vesicles that contain Hh (Figure 3A and Supplemental Video S1) compared with the relatively small punctae of Hrs observed in untransfected cells (Supplemental Figure S3A). To examine whether MVBs harbor Hh-containing vesicles, we directly tracked the fate of endocytosed Hh from the cell surface into compartments that contain the late endosome (LE)/MVB marker lysosome-associated membrane protein (LAMP; Lawrence *et al.*, 2010; Swetha *et al.*, 2011). Endocytosed Hh colocalized with only the vesicular aspect of the tubulovesicular LAMP-GFP–containing structures (Figure 3B and Supplemental Video S2). The most prominent role of MVBs is in facilitating the degradation of internalized cargo and the ILV components by their fusion with lysosomes (Fader and Colombo, 2009), which tend to be tubular in insect cell lines (Sriram *et al.*, 2003; Swetha *et al.*, 2011).

To explore the fate of Hh-containing MVBs, we tracked the HhmCFP (monomeric cyan fluorescent protein [mCFP] tagged to Hh) fusion protein in live endocytic assays. Tetramethyl rhodamine–conjugated dextran (TMR-Dex), a fluid-phase marker, is delivered to tubular lysosomes in a 2-h endocytic pulse in hemocytes and S2R+ cells (Sriram *et al.*, 2003; Swetha *et al.*, 2011). When TMR-Dex was cointernalized with Alexa 647–labeled anti–GFP Fab (A647–anti-GFP Fab) in HhmCFP-transfected cells, we observed considerable colocalization of both the probes in vesicular structures, but, once again, HhmCFP was absent from the tubular lysosomes outlined by endocytosed TMR-Dex (Figure 3C).

In a parallel experiment, endocytosed GFP-GPI (GFP tagged glycosylphosphatidylinositol; labeled by A647–anti-GFP Fab) was detected in tubular structures marked by TMR-Dex (Figure 3D). This suggests that although endocytosed membrane proteins may be detected in the tubulovesicular aspect of the late endosomal system, endocytosed Hh accumulates in the lumen of the vesicular aspect of this endosome but fails to be delivered to the tubular aspects of the lysosomal system. To further characterize the localization of HhGFP in the endolysosomal system, we used immuno-EM to detect the contents of the lumenal aspects of these organelles. HhGFP was clearly detected in the lumen of an MVB, as indicated by the presence of gold particles labeling small ILVs inside the MVB (Figure 3E).

Extracellular vesicles containing Hh with the right topology can also be generated by direct budding from the plasma membrane using a mechanism similar to that used by enveloped viruses (Meiser *et al.*, 2003), without any requirement for endocytic trafficking of Hh. To test whether the Hh exovesicles are indeed released from an endocytosed vesicular pool or directly from the cell surface, we perturbed two key trafficking mediators—*Drosophila* Rab5 (*d*Rab5), a regulator of the early endocytic pathway (Bucci *et al.*, 1992), and Shibire, *Drosophila* dynamin, which controls internalization at the cell surface. Expression of dominant-negative form of *d*Rab5 in the Hh-producing domain in the wing imaginal disc has been shown to have an effect on the signaling range of Hh (Callejo *et al.*, 2011), whereas loss of Shibire function leads to extracellular accumulation of Hh in its producing domain in the apical regions of the wing imaginal disc (Ayers *et al.*, 2010; Callejo *et al.*, 2011). RNA interference (RNAi)–mediated knockdown of *d*Rab5 and Shibire resulted in a significant reduction in the levels of HhGFP in the P100 and the P250 fractions (Figure 3, F and G). The depletion of *d*Rab5 and Shibire resulted in expected effects on endocytosis, consistent with their roles in different legs of the endocytic process—endosomal dynamics (*d*Rab5) and internalization (Shibire). *d*Rab5 depletion caused a reduction in the fluid-phase uptake (Supplemental Figure S3B) and a decrease in size of Hh-containing endosomes (Supplemental Figure S3, C–E). Shibire knockdown resulted in a reduction in the uptake of transferrin receptor (TfR; Supplemental Figure S3F) and enhanced uptake of the fluid phase (Supplemental Figure S3G). Of importance, Shibire depletion enhanced the levels of HhGFP at the cell surface in S2R+ cells (Supplemental Figure S3, H and I) suggesting its role in internalization of Hh.

Although Shibire and *d*Rab5 affect different steps in internalization of Hh, a decrease in Hh secretion could have resulted from

TMR-Dex. Scale bar, 2 µm. (D) Unlike Hh-mCFP, endocytosed GFP-GPI (single confocal slice) visualized with a 2-h endocytic pulse of A647–anti-GFP Fab and imaged using an FV1000 confocal microscope is visualized in both tubular and vesicular structures of GFP-GPI–expressing S2R+ cells. Scale bar, 2 µm. (E) Immuno-EM on frozen sections from S2R+ cells transfected with HhGFP show labeling on the ILVs inside the MVB lumen, detected using the anti-Hh antibody and probed using 10-nm protein A–gold. (ii) Zoomed image of the MVB marked in (i); (iii, iv) other representative images of MVBs from different sections. Scale bar, 200 nm. (F, G) Western blots (F) show the amount of HhGFP in the corresponding cellular (Cells) and secreted fractions (P100, P250) obtained from HhGFP-transfected S2R+ cells treated with control (Zeocin) or with indicated RNAi after being subjected to the same sedimentation scheme shown in Figure 1A. Black vertical lines denote deletion of other lanes from the blots containing biological replicates of the same experiment. (G) Bar graph shows the extent of reduction in the amount of secreted HhGFP in P100 and P250 fractions (represented as percentage reduction in normalized secretion with respect to control; red dashed line) in the indicated RNAi treatment determined after quantifying the density of the staining in the Western blots. Nonsaturating exposures of cellular, P100, and P250 fractions were used for intensity measurements, and values in P100 and P250 fractions were normalized to the values in cell lysates. Data from at least three independent experiments are expressed as mean ± SD; $*p < 0.05$, $**p < 0.01$, $***p < 0.001$. (H) Western blots reflect the amount of HhGFP in the cellular (Cells) and secreted (P100, P250) fractions derived from HhGFP-transfected S2R+ cells treated with control and *d*Rab27 RNAi. Black vertical lines denote deleted regions from the blot. Deleted lanes had biological replicates and samples described elsewhere (Vps28 RNAi; Figure 6F). (I) Bar graph showing extent of secretion of ss-HRP expressed in S2R+ cells transfected with pMT-ss-HRP and treated with indicated RNAi compared with control RNAi (red dashed line). Data from two independent experiments. Note the extent of reduction in ss-HRP secretion in *d*Rab35 RNAi treatment vs. the lack of any change in *d*Rab27.

indirect effects. If traffic to MVBs is essential for exovesicular release of Hh, a block in MVB fusion to the plasma membrane should affect Hh secretion. Rab27 and Rab35 are two Rab proteins implicated in the fusion of a MVB to the plasma membrane (Hsu *et al.*, 2010; Ostrowski *et al.*, 2010), which would be important for release of ILVs as exovesicles. RNAi against *Drosophila* Rab27 (*d*Rab27) resulted in reduction of Hh in both the P100 and P250 exovesicular fractions (Figure 3, G and H). Of importance, depletion of *d*Rab27 did not significantly affect the secretion of secretory horseradish peroxidase (ss-HRP), which follows a conventional secretory route (Bard *et al.*, 2006), indicating that this protein is not important for conventional exocytic transport (Figure 3I). RNAi against *Drosophila* Rab35 (*d*Rab35) affected secretion of ss-HRP (Figure 3I), and hence we did not pursue it further for its effects on exovesicular secretion of Hh. These results provide evidence for the role of endocytic machinery in delivery of Hh to the MVB lumen and the subsequent fusion of MBVs to the plasma membrane in exovesicular secretion.

Oligomerization of Hh is necessary for its exovesicular release

We previously showed that Hh forms dense oligomers mediated via an electrostatic interaction between Hh monomers and that this oligomerization is necessary for its long-range signaling. These conclusions were derived by using an oligomerization-defective Hh mutant, the HhK132D variant (Vyas *et al.*, 2008), ectopic expression of which fails to elicit long-range target-gene activation. Recent studies show that perturbations in ESCRT proteins in the Hh-producing domain also affect long-range signaling in the wing imaginal disc (Gradilla *et al.*, 2014; Matusek *et al.*, 2014). To explore the role of oligomerization of Hh in the generation of the long-range carriers, we expressed mCFP-tagged HhK132D (HhK132DmCFP) in S2R+ cells and measured the extent of exovesicular release of Hh. In comparison with wild-type Hh, the HhK132DmCFP protein was secreted very poorly in both fractions, as detected by quantitative Western blotting (Figure 4, B and C), and there was an almost complete absence of the larger vesicle by FCS measurements on the GFP variant of this protein (Figure 4, D and E, and Table 2).

Because Hh exhibits a hierarchical organization in which its oligomerization is a prerequisite for its interaction with heparan sulfate proteoglycans (HSPGs; Vyas *et al.*, 2008), we asked whether HSPG interaction was important for incorporation into exovesicles. For this purpose, we used a different Hh variant, HhΔCWmCFP (mCFP tagged to HhΔCW), in which the Cardin–Weintraub (CW) domain necessary for interaction with HSPGs is deleted but the protein retains its ability to form nanoscale clusters (Vyas *et al.*, 2008). In contrast to the oligomerization-defective variant, expression of HhΔCWmCFP protein resulted in a quantitative increase in secretion compared with its wild-type counterpart (Figure 4, B and C). The secreted forms of Hh also exhibited a distribution of the two distinct diffusing species as detected by FCS, comparable to the wild-type protein (Figure 4, D and E, and Table 2). Thus incorporation of Hh into exovesicles is likely to be independent of its ability to interact with HSPGs.

Oligomerization-defective Hh is impaired in its endocytic delivery to MVBs

To explore the reason behind impairment in exovesicle secretion of the oligomerization-defective mutant, we tested two possibilities, each of which could independently lead to a defect in exovesicular release: one in which the mutant protein may be recycled to the cell surface directly from the early endosome (EE) without reaching the MVBs, and the other in which the oligomerization-defective mutant could have a lower endocytic capacity, resulting in impaired delivery to the MVB lumen (Figure 5A).

When the fate of endocytosed HhK132DmCFP was tracked, it entered endosomes that colocalized with LAMP-GFP (Figure 5B), and also exhibited enlarged Hrs-labeled endosomal structures similar to the HhGFP (Figure 5C). Further, electron micrographs showed that the mutant was equally visualized in the MVB lumen on ILVs (Figure 5D). However, the overall level of the protein in the endosome was significantly reduced in the Hh mutant, suggesting impairment in endocytosis. This was confirmed by a direct measurement of endocytosis of HhK132D in comparison with the wild-type counterpart by a surface accessibility assay (Guha *et al.*, 2003). Our results showed that the oligomerization-defective mutant was severely impaired in its ability to be endocytosed compared with the wild type (Figure 5E), suggesting that the extent of endocytosis into MVBs appears to be a major determinant for exovesicular secretion. Consistent with this hypothesis, HhΔCWmCFP, which shows increased exovesicular secretion, has increased endocytic capacity (Figure 5E). Taken together, these results show that both extent of endocytosis and subsequent transfer to the ILVs are likely to regulate exovesicular generation and release.

Perturbations in ESCRT proteins result in intracellular Hh accumulation and affect its exovesicular secretion

To determine the mechanism of Hh exovesicle generation, we examined cellular pathways involved in MVB biogenesis. This has been shown to proceed via an ESCRT-dependent pathway (Vaccari *et al.*, 2009; Henne *et al.*, 2013), as well via an ESCRT-independent pathway that is dependent on the sphingolipid ceramide (Trajkovic *et al.*, 2008). Furthermore, recent results indicate that Hh secretion likely involves molecules of the ESCRT machinery (Gradilla *et al.*, 2014; Matusek *et al.*, 2014). Hence we revisited the role of a subset of components of the ESCRT machinery in MVB-dependent exovesicle generation.

RNAi against ESCRT proteins Vps28 (ESCRT1), Shrub (ESCRT3), and Vps4 (accessory protein) resulted in reduction of their respective protein/mRNA levels in cells (Supplemental Figure S5A). In addition, we saw an intracellular accumulation of endogenous Hrs (ESCRT0) in the cells upon Shrub and Vps4 RNAi treatments, suggesting a block in MVB biogenesis in these conditions (Figure 6A). To test these observations in the wing imaginal disc, we expressed Shrub RNAi using Apterous-Gal4 in the dorsal region, leaving the ventral region unaffected. Not only did we observe Hrs accumulation in the dorsal regions, but the Hrs punctae also stained positive for LE marker *Drosophila* Rab7 (*d*Rab7), confirming them as endocytic intermediates (Figure 6D and Supplemental Figure S4C). We observed accumulation of Hh in Hrs-containing structures in both Shrub and Vps4 RNAi–expressed wing imaginal discs using Apterous-Gal4 (Figure 6, B and C, and Supplemental Figure S4, A and B). This accumulation was detected in both the posterior and the anterior regions of the wing imaginal disc. Whereas accumulation of Hh in the anterior could be due to a defect in degradation due to aberrant MVB biogenesis, the accumulation in the posterior domain is unlikely due to a defect in degradation, since null clones of Deep orange, a protein involved in lysosomal biogenesis, leads to Hh accumulation in the anterior but not in the Hh-producing domain (Callejo *et al.*, 2011; D'Angelo *et al.*, 2015).

Of significance, RNAi against Vps28, Shrub, and Vps4 in cells resulted in decreased release of HhGFP in P100 and P250 fractions (Figure 6, E and F). The decrease in Hh secretion in ESCRT RNAi depletions could have resulted from a nonspecific effect on the general pathway of protein secretion by the perturbation of MVB

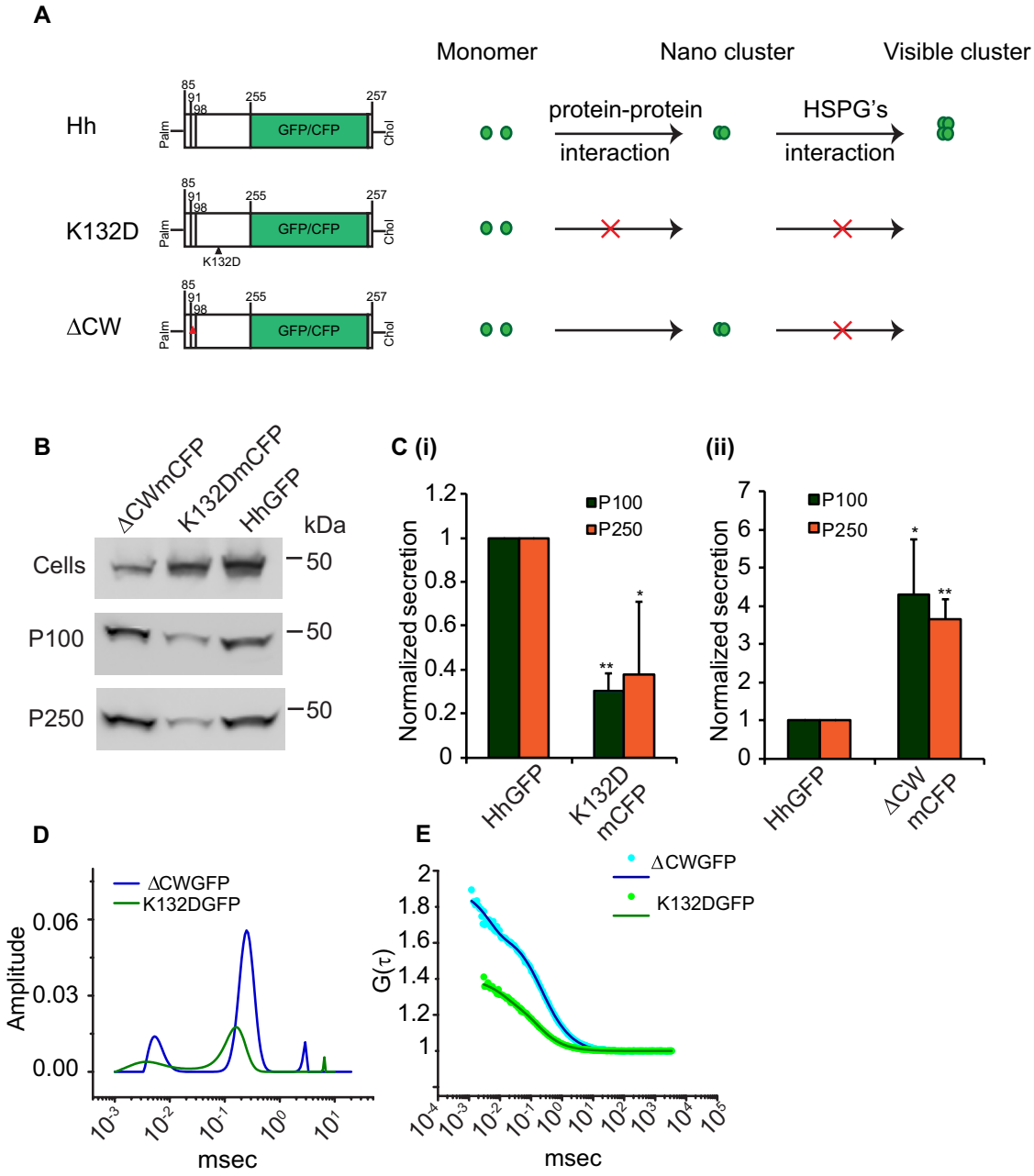

FIGURE 4: Oligomerization of Hh is necessary for its vesicular release. (A) Cartoon representing different Hh variants with respective mutations used to gain mechanistic insights into the role of Hh organization in its secretion. Hh forms a nanoscale cluster on the cell surface through a protein–protein interaction, which is in turn essential for formation of optically resolvable clusters in association with HSPGs. A point mutation, K132D, results in disruption of an electrostatic interaction between Hh monomers that abolishes the hierarchical Hh clustering, whereas upon deletion of the HSPG-interacting CW (residues 91–98) domain it retains its ability to oligomerize at the nanoscale but cannot form optically resolvable clusters. (B, C) Western blots (B) reflect the amount of protein in the cellular (Cells) and secreted fractions (P100 and P250) of HhGFP, HhK132DmCFP, and HhΔCWmCFP expressed in S2R+ cells. (C) Bar graphs quantify the extent of secretion of HhK132DmCFP (i) and HhΔCWmCFP (ii) in both P100 and P250 fractions as compared with HhGFP. Nonsaturating exposures of cellular, P100, and P250 fractions were used for intensity measurements, and values in P100 and P250 fractions were normalized to the values in cell lysates. Data represent mean ± SD from three experiments; *$p < 0.05$, **$p < 0.01$. (D, E) Graphs showing distributions of diffusion time scales (D) of the different species present in the P100 fractions from S2R+ cells expressing HhK132DGFP (K132DGFP; green) and HhΔCWmCFP (ΔCWmCFP; blue) derived from the autocorrelation analysis of FCS data (E, dotted lines), using the MEM fitting routine as described in Figure 1 and used to compute the two-component, 3D diffusion fit of the FCS traces (solid lines in E).

Hh variant	D_1 (μm²/s)	Fraction (%)	D_2 (μm²/s)	Fraction (%)
HhΔCWGFP	40.6 (± 2.77)	86.2 (± 3.6)	6.44 (± 1.62)	13.8 (± 3.6)
HhK132DGFP	50.5 (± 4.14)	96.7 (± 0.8)	1.99 (± 1.11)	3.7 (± 0.8)

Diffusion coefficients and fractions obtained after fitting the FCS data to a two-component, 3D diffusion fit for measurements made on P100 for the two Hh variants. There is almost complete absence of the slow-diffusing form in P100 for the oligomerization-deficient HhK132DGFP form. The HSPG-binding-deficient mutant of Hh, HhΔCWGFP, is secreted in two diffusible forms, comparable to HhGFP.

TABLE 2: FCS measurements on P100 fraction of Hh variants.

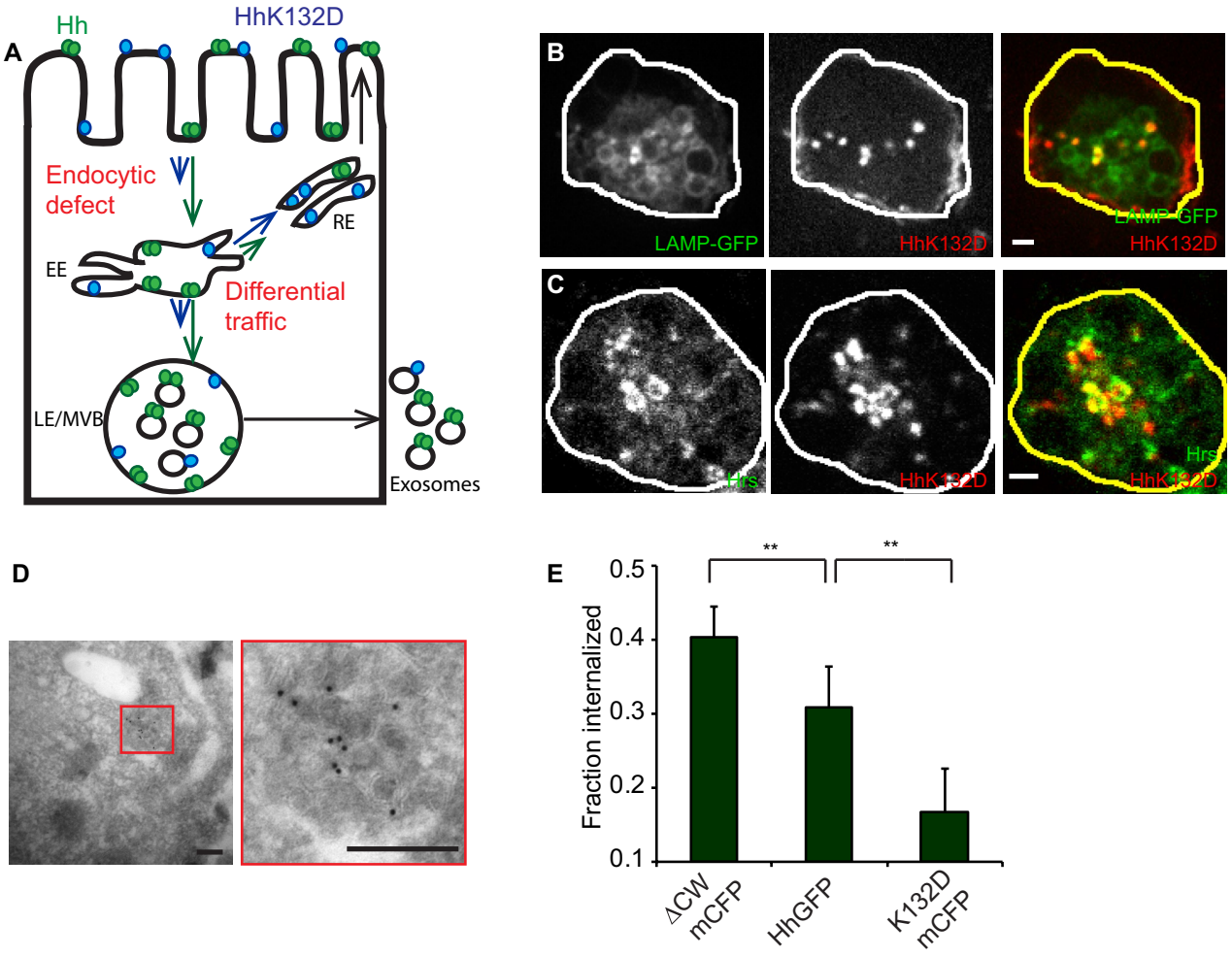

FIGURE 5: Oligomerization-defective Hh is impaired in its endocytic delivery to the MVBs. (A) Model to explain the differences in trafficking of Hh variants to account for observed differences in secretion. Hh is represented in green as a homo-oligomer, and K132D is shown in blue in a monomeric form. The lengths of the arrows reflect the extent of traffic for each variant in a particular pathway. The extent of partitioning toward the recycling pathway of the Hh variants vs. the late endosomal pathway regulate delivery to the MVB and hence result in modulation of ILV formation. Alternatively, a more upstream endocytic block could also lead to similar consequences. (B, C) S2R+ cells expressing HhK132DmCFP were incubated with A647–anti-GFP Fab (red in merge) for 20 min (B) or 2 h (C) to localize internalized protein. It colocalizes with LAMP-GFP (B; green in merge) coexpressed in the same cells or with immunodetected Hrs (C; green in merge). Single confocal slices are shown from cells imaged using a PerkinElmer spinning-disk confocal microscope (B) or an Olympus FV1000 confocal microscope (C). Note that HhK132DmCFP traffics to LE/MVB structures and results in a redistribution of Hrs. Scale bar, 2 μm. (D) HhK132DmCFP is also visualized on ILVs inside the MVB lumen in cryosections of cells transfected with HhK132DmCFP labeled using anti-GFP antibody and detected using a 10-nm gold–conjugated secondary antibody. Scale bar, 200 nm. (E) Bar graphs showing the fraction of the surface-bound A647–anti-GFP Fab internalized in a 10-min endocytic pulse using a surface accessibility assay for each of the indicated Hh variants. Data from two experiments are represented as mean ± SEM from at least 50 cells for each variant; $^{**}p < 0.01$.

biogenesis. To rule out this possibility, we directly measured the effect of RNAi on the secretion of a secretory marker ss-HRP. Our results show that RNAi-mediated depletion of Vps4, Vps28, and Shrub did not reduce ss-HRP secretion, indicating that conventional protein secretion was not hampered in our experiments (Supplemental Figure S5E). Furthermore, we also observed that depletion of Shrub causes a reduction of signaling ability of the P100 and P250 pellets (Supplemental Figure S5B).

Taken together, these results suggest that ESCRT proteins Vps28 and Shrub and the regulatory proteins Vps4 and Alix (Supplemental Figure S5, C and D) have an effect on MVB biogenesis and affect the exovesicular release of Hh by trapping it intracellularly in vesicular structures.

Perturbations of ESCRT proteins affect Hh spread and the signaling output in the *Drosophila* wing imaginal disc

At the level of light microscopy, extracellular staining of Hh revealed a punctate distribution in the wing imaginal disc, with significant enrichment along the dorsoventral boundary in the anterior region, as observed previously (Ayers *et al.*, 2010). Moreover, Hh puncta in this region, as well as in other regions from the wing imaginal disc, colocalized with Hrs (Supplemental Figure S6, A and B), an exovesicular marker also used in our biochemical experiments, consistent with generation of Hh-containing exovesicles in the *Drosophila* wing imaginal disc. Hh was also visualized in MVBs by immuno-EM inside cells of the wing imaginal disc epithelium (Supplemental Figure S6C).

Because a subset of ESCRT proteins had an effect on the MVB biogenesis and thereby exovesicular secretion of Hh in cell-based assays, we reasoned that perturbations in the ESCRT proteins should affect the spread of Hh in the anterior domain. When we stained for extracellular Hh in control and Shrub RNAi–expressing discs driven using Hh-Gal4, we found that the spread of extracellular Hh was significantly reduced in the anterior regions of the wing imaginal disc in the Shrub RNAi–expressed discs (Figure 7, A–C).

To test the role of exovesicles in signaling, we asked whether perturbation of ESCRT proteins in the Hh-producing domain could have an effect on Hh signaling in the anterior domain of the wing imaginal disc. Hh signaling leads to the stabilization of Ci, which can be detected based on its intense staining compared with the low levels of the truncated form of Ci (Méthot and Basler, 1999). The length of the Ci-155 staining band is therefore a measure of the long- range spread of Hh. Hh signaling also leads to activation of short-range targets such as Engrailed and Ptc, intermediate-range targets such as Collier (Col), and other long-range targets, such as Decapentaplegic (Dpp) and Iroquois (Torroja *et al.*, 2005). We used the staining patterns of the long-range Dpp-LacZ and Ci and the short- and intermediate-range Ptc and Col, respectively, as readout for Hh signaling in context of perturbations of the proteins of the ESCRT machinery. RNAi against the ESCRT components was expressed in the Hh-producing domain using Hh-Gal4, and the signaling outputs of Dpp, Ci, Ptc, and Col were measured. We found a significant reduction in the expression range of the Dpp-LacZ (Figure 7, D–F and J) and the Ci-155 form (Figure 7, G–I and K) in both Shrub RNAi and Vps4 RNAi expression, whereas we observed no significant difference in the extent of short-range Ptc expression (Supplemental Figure S7, A–C and G) or intermediate-range target Col (Supplemental Figure S7, D–F and H). Thus perturbations of ESCRT proteins in the Hh-producing domain affect its spread in the anterior domain and long-range signaling in the wing imaginal disc, consistent with the idea that Hh exovesicles are mediators of long-range signaling.

DISCUSSION

Cell fate–determining secretory morphogens travel over several cell distances, effecting graded signaling responses at different distances from the producing location. Hh is a canonical example of this type of morphogen, and studies with this morphogen have uncovered new paradigms. In earlier work from our laboratory, we found that Hh forms dense oligomers that are necessary for long-range signaling; oligomerization-defective Hh variants were unable to participate in long-range signaling. However, the nature of the secreted morphogen that was responsible for the long-range signals was elusive. Here our studies addressed the nature of the long-range signaling vehicle used by Hh, using a two-pronged approach. First, we addressed the nature of secreted forms of Hh by expressing the protein in an appropriate insect cell system (S2R+ cells) and characterizing the biochemical, biophysical, and morphological nature of the secreted forms, elucidating the molecular machinery involved in generating them. Second, we followed this with pertinent perturbations in the developing wing imaginal disc system of the fruit fly, where the range of the signaling response has been best studied (Panáková *et al.*, 2005; Torroja *et al.*, 2005; Ayers *et al.*, 2010), to provide a functional context for the results from the cell-based system.

Nature of the exovesicles

Our biochemical, biophysical, and morphological studies revealed that Hh is packaged into a set of membrane-bound vesicles that have the same density of canonical exovesicles (1.10–1.2 g/ml) but are present as at least two signaling-competent forms as revealed by the differential centrifugation protocol we developed. The larger form is more pleiomorphic (40–100 nm) and, as expected, sediments at lower *g*-force (P100). It also cosediments with a proteins of the ESCRT machinery (Hrs, Vps28) and typical membrane proteins (Lbm, Stx1, TfR) often found in many exovesicular preparations (Koles *et al.*, 2012; Beckett *et al.*, 2013). The smaller, more homogeneous form (20–40 nm; P250) sediments with only a subset of the ESCRT machinery (Hrs, Vps28) and lacks many of the typical membrane markers of exovesicles. This clearly indicates heterogeneity of morphological forms that carry Hh. It is conceivable that the P100 form does carry additional cargo and hence has a different functional role.

The presence of Hh in both fractions and on the two types of vesicles is unlikely to be an artifact of overexpression of an ectopic protein, since, when we express another lipid-anchored protein, the glypican Dally (Khare and Baumgartner, 2000), in S2R+ cells, it is detected only in the P100 fraction (unpublished data). These observations raise the issue of whether differences observed in protein composition between small and large exovesicles are due only to a size constraint or whether specificity is involved in packaging. Our results suggest that there could be a combination of both factors, which needs to be explored further, along with the importance of these different-sized vesicles in context of Hh signaling and also in exosome functions in other signaling contexts. Indeed, in a similar fractionation protocol for purifying Sonic Hedgehog–containing vesicles, Vyas *et al.* (2014) showed that the two vesicular forms differentially regulate the conversion of embryonic stem cells to motor neurons. However, at this stage, it is unclear whether the molecular compositions of the two forms are very different, since cosedimentation does not confirm cohabitation in the same membrane-bound vesicle. The potential presence of Dally in the P100 sedimentable exovesicles could be important for more effective binding of these vesicles to cytonemes, decorated by Interference hedgehog and Brother of interference

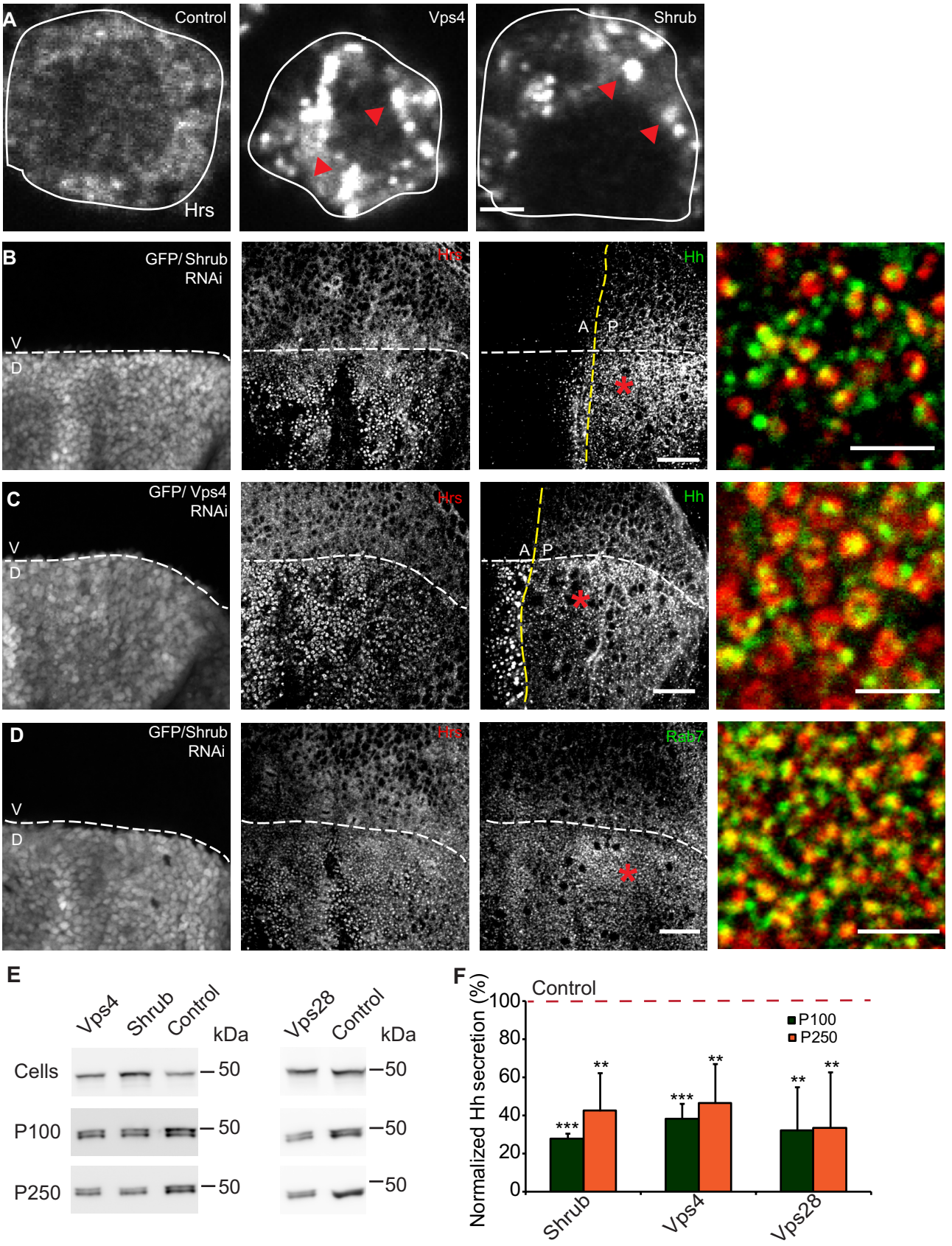

FIGURE 6: Perturbations in ESCRT proteins result in intracellular Hh accumulation and affects its exovesicular secretion. (A) Endogenous Hrs (ESCRT 0; red arrowheads) immunostained using anti-Hrs antibody accumulates in vesicular structures in S2R+ cells upon Shrub (ESCRT3) and Vps4 RNAi treatments compared with treatment of cells using a control RNAi. Scale bar, 2 μm. (B, C) *Drosophila* wing imaginal discs from animals expressing Shrub RNAi (B) or Vps4

hedgehog (Bischoff *et al.*, 2013; Gradilla *et al.*, 2014), as Dally has been shown to interact with these molecules in the wing imaginal discs (Bilioni *et al.*, 2013).

The exovesicles that we characterize here are unlikely to be the same as the lipophorin-associated particles isolated earlier (Panáková *et al.*, 2005) because when cells were grown in a medium completed depleted of 250,000 × *g* sedimentable material or grown in the absence of serum (medium devoid of any lipoproteins), the two exovesicular forms of Hh were still produced from the cells. A third form of secreted Hh (S250) was indistinguishable from a monomer/dimer of HhGFP in FCS measurements (and is unlikely to be associated with any membrane since it does not sediment even at 250,000 × *g*). This form may be derived from a processing activity that is present in the extracellular serum–containing medium and is not generated by the cells when grown in serum-free medium. We did not study this form further.

In summary, we isolated a population of Hh-containing exovesicles that are very heterogeneous in size but carry the signature of exosomes, with the presence of ESCRT machinery indicating subpopulations with overlapping biochemical compositions.

Endocytosis of oligomeric Hh is necessary for the generation of Hh exovesicles in a MVB-dependent manner

The presence of Hh inside MVBs and the perturbation of exovesicular release by the depletion of components of the ESCRT machinery, which facilitates ILV generation, argue that Hh may be delivered via endocytosis to the MVB. Indeed, affecting the endosomal properties of Hh by perturbing *d*Rab5 function drastically reduced exosomal release of Hh. Similarly, knockdown of Shibire, which results in extracellular accumulation of Hh, also reduced exovesicular release of Hh, thus suggesting a direct role of Hh endocytosis in exovesicular release.

Finally, after the delivery of Hh to the MVBs from the cell surface, it is important for MVBs to fuse to the plasma membrane to release ILVs in the form of exovesicles. For this purpose, S2R+ cells seem to use *d*Rab27, as perturbation in this Rab protein has been previously shown to be important in the process of MVB fusion (Ostrowski *et al.*, 2010). This emphasizes that endocytic delivery to the MVBs is required for loading Hh onto exovesicles rather than a requirement of rerouting it to other membrane domains for exovesicular secretion (D'Angelo *et al.*, 2015). However, *d*Rab27 is absent in the *Drosophila* wing imaginal disc (Chan *et al.*, 2011), and hence we could not test the effects of this protein in the animal. There is a possibility of another Rab protein that could take over the MVB fusion function in the wing imaginal disc, which needs to be identified. Taken together, these observations indicate that generation of Hh-containing exovesicles requires delivery of Hh into MVBs. Recent studies that suggest ESCRT-dependent surface blebbing may account for the generation of exovesicles (Matusek *et al.*, 2014). However, our results on the intracellular trafficking of Hh in S2R+ cells to MVBs, as well as its accumulation in Hh-producing cells in endocytic structures when Vps4 and Shrub are perturbed, suggest that ESCRTs act at the level of MVB biogenesis, where Hh is packaged into ILVs for exovesicular delivery, and surface blebbing, which can contribute vesicles with a similar morphology as exovesicles, is unlikely to have a role in the process.

Consistent with a role for endocytosis in generation of ILVs, we find that efficient endocytosis of Hh is necessary for its subsequent packaging into MVBs. The nanoscale clustering of numerous lipid-anchored proteins, such as GPI-anchored proteins, and toxins that bind to lipid-anchored receptors (Shiga and cholera toxin) has been suggested as a sorting signal for endocytosis of these molecules via clathrin-independent pathways (Johannes and Mayor, 2010). Consistent with these ideas, oligomerization-defective HhK132D mutant is poorly endocytosed and has a defect in exovesicular secretion, whereas variants of Hh that retain their oligomerization capacity (HhΔCW and Hh) are efficiently endocytosed and secreted. Thus the endocytic efficiencies of Hh and its variants correlate with the capacity for Hh exovesicle secretion; lower and higher endocytosis of HhK132D and HhΔCW, respectively, map coherently to their capacity to be secreted as exovesicles. In addition, the enhanced endocytic capacity of the HSPG-interaction-defective but oligomerization-competent HhΔCW mutant (Vyas *et al.*, 2008) also suggests that association with cell surface HSPGs may act to inhibit the extent of endocytosis of Hh and therefore modulate its exovesicular secretion.

Implications for signaling

Our results have a direct bearing on the form of Hh to participate in long-range signaling. Any perturbation of Hh exosome production—for example, by inhibiting the ESCRT proteins or creating the oligomerization-defective HhK132D (Vyas *et al.*, 2008)—affected long-range signaling and retained the ability to signal at a short range. A close examination of the signaling data on the wing imaginal disc in which ESCRT functions had been perturbed showed that along with the reduction in the range of Hh delivery, there was a drastic reduction of Dpp and Ci155 induction. However, both short (Ptc) and intermediate (Col) targets are unaffected. Surprisingly, the slope of the Hh gradient in regions adjoining the anterior/posterior (A/P) boundary, where Hh activates high-threshold targets, is unaltered, but the amount of Hh is dramatically reduced in regions further away from the axis, where Hh activates low-threshold targets such as Dpp. This segregation suggests the requirement for two mechanisms—one for

RNAi (C) under the control of Apterous-Gal4, marked by GFP fluorescence in the dorsal region, result in the local accumulation of Hh (green in merge) in large Hrs-positive (red in merge) compartments in the apical/subapical planes derived from a 3D stack of confocal images of the wing imaginal disc. Scale bar, 20 µm. Asterisk indicates regions from the posterior that are shown at a higher magnification. Scale bar, 5 µm. (D) Dorsal regions of *Drosophila* wing imaginal discs expressing Shrub RNAi driven using Apterous-Gal4 similar to B and marked by GFP fluorescence show that Hrs puncta (red in merge) stain for LE marker *d*Rab7 (green in merge), confirming them as endocytic intermediates. Scale bar, 20 µm. Asterisk indicates a region that is shown at a higher magnification. Scale bar, 5 µm. (E) Western blots (top) reflect HhGFP in cellular (Cells) and secreted (P100 and P250) fractions (middle and bottom) derived from S2R+ cells transfected with HhGFP and grown in the presence of the indicated RNAi against ESCRT proteins and Vps4. (F) Bar graph showing the extent of reduction in normalized secretion (with respect to the control; red dashed line) of HhGFP in the P100 and P250 fractions in each of the indicated RNAi treatments. Nonsaturating exposures of cellular, P100, and P250 fractions were used for intensity measurements, and values in P100 and P250 fractions were normalized to the values in cell lysates. Data, expressed as mean ± SD, were derived from at least four independent experiments; $*p < 0.05$, $**p < 0.01$, $***p < 0.001$.

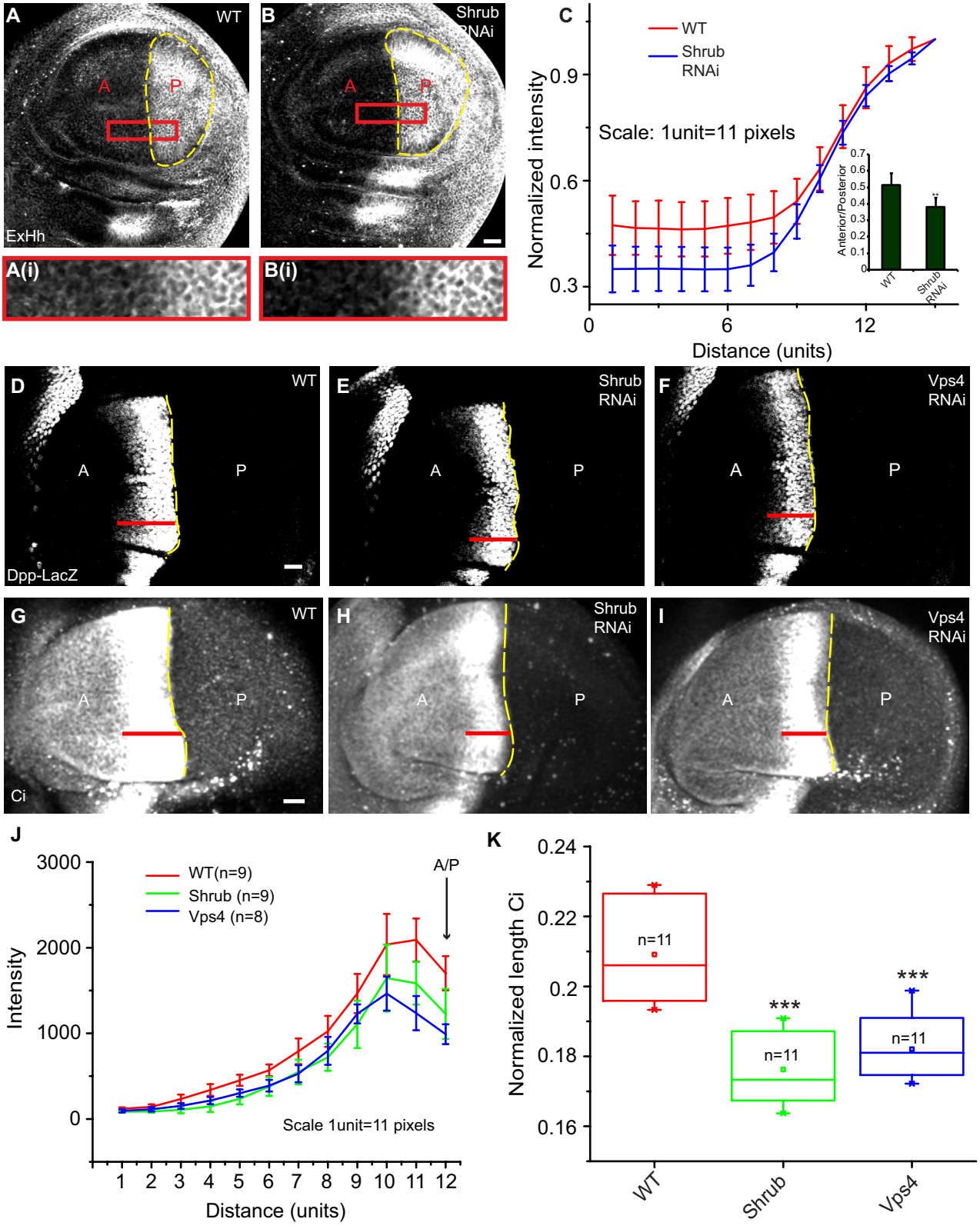

FIGURE 7: Perturbations of Shrub and Vps4 proteins affect Hh spread and its signaling output in the wing imaginal disc. (A, B) *Drosophila* wing imaginal discs stained for extracellular Hh (ExHh) from WT (A) and animals expressing Shrub (B) RNAi under the control of Hh-Gal4, marked using the yellow dashed lines, show a reduction in spread of Hh in the anterior domain in RNAi-treated discs. Images were subjected to median filtering before representation. Scale bar, 20 μm. Outlined regions are shown at a higher magnification. (C) Quantification shows a reduction in the spread of extracellular Hh in Shrub RNAi–treated discs compared with the WT control. The line represents an averaged trace from seven wing imaginal discs in each condition. Graph in the inset shows a reduction in anterior/posterior ratio of Hh intensities in Shrub RNAi. Data are represented as mean ± SD from seven wing imaginal discs for each condition;

Hh-containing exovesicles in spreading at a long range and another for activating the high-threshold genes abutting the A/P axis. In apparent contradiction to our results, previous studies showed that loss of Shibire function in the wing imaginal disc actually leads to expansion of long-range targets due to the accumulation of surface Hh being transported using a proposed complex containing Hh and the glypicans aided by the hydrolase Notum (Ayers *et al.*, 2010). The presence of distinct modalities in Hh transport makes it difficult to comment on the mechanisms of secretion by just measuring target-gene activation in the wing imaginal disc, and hence the use of cellular assays and direct visualization of the nature of the Hh carriers would be necessary to resolve these discrepancies.

Conclusions

Taken together, these observations suggest a mechanism for Hh secretion and signaling. Hh is secreted on exovesicles derived via endocytic accumulation of Hh in ILVs inside MVBs. Their subsequent fusion at the cell surface releases Hh-containing exovesicles to carry out long-range signaling. The endocytic receptor involved in Hh delivery to the MVB, as well as the role of clustering in endocytosis, remains uncharacterized. A recent study indicates that interaction of Hh with Dispatched is necessary for its endocytosis (D'Angelo *et al.*, 2015), which in turn could lead to Hh delivery into MVBs. The generation of exovesicles adds to the multiplicity of machinery already available for long-range Hh transport. Exosome-based signaling allows a distinct regulation of long- and short-range targets, as is evident from the differential effects of perturbations on the signaling readout from Hh. Such a mechanism also exists for another secreted morphogen, Wg, in which Reggie1/Flotillin2-dependent carriers of Wg are important only for long-range signaling (expression range of Distalless) but does not affect the expression of its short-range target Senseless (Katanaev *et al.*, 2008), suggesting a more general principle for the differential regulation of short- and long-range signaling.

MATERIALS AND METHODS

Cell culture and transfections

S2R+ cells were cultured in Schneider's medium (Life Technologies/Invitrogen, Carlsbad, CA) supplemented with 10% heat-inactivated fetal bovine serum (FBS; Life Technologies/Invitrogen), 100 µg/µl penicillin, 100 µg/µl streptomycin, and 750 µg/µl L-glutamine (SCM). Cells were maintained at 23°C. Clone8 cells were grown in Complete M3 medium, which comprises Shields and Sang M3 insect medium (Sigma-Aldrich, St. Louis, MO) along with 2% heat-inactivated FBS, 2.5% fly extract, 0.5 mg/ml insulin (Sigma-Aldrich), 100 µg/µl penicillin, and 100 µg/µl streptomycin. Transfections were carried out using Effectene reagent (Qiagen, Hilden, Germany) for both cell types and according to manufacturer's protocols for S2R+ cells. The Effectene amount was reduced fivefold for transfection of Clone8 cells.

Vesicle isolation

To isolate exovesicles, cells were grown in exosome-harvesting medium, which consists of Schneider's medium and 10% heat-inactivated FBS subjected to 16 h of spin at 150,000 × *g* at 4°C. After cells were grown in this medium, the conditioned medium was removed and spun at low speed at 800 × *g* for 30 min at 4°C to remove large cellular debris. The resulting supernatant was passed through a 0.22-µm membrane filter and then spun at 100,000 × *g* using a TLA-45 rotor at 4°C for 2 h in an Optima MAX-XP ultracentrifuge (Beckman Coulter, Brea, CA) to obtain the P100 fraction. The supernatant of this fraction was subsequently spun down at 250,000 × *g* in the same centrifuge using a TLA-100.3 rotor at 4°C for 2 h obtain P250. Pellets obtained in both steps were washed using Tris-HCl–buffered saline or phosphate-buffered saline (PBS) and resuspended in the same buffer before being taken for Western blots, immuno-EM, and FCS measurements. The medium preclearing was also done using subsequent centrifugation steps of 2000 × *g* and 10,000 × *g*, followed by the same high-speed centrifugation protocol.

Sucrose gradient centrifugation

For sucrose gradient centrifugations, P100 and P250 pellets were resuspended and loaded on the top of a linear sucrose gradient (0.25–2 M; Stoeck *et al.*, 2006; Gross *et al.*, 2012) and spun down at 210,000 × *g* for 16 h at 4°C. Ten fractions were collected from top of the gradient, and their densities were measured using a refractometer. For concentrating proteins, the fractions were subjected to chloroform–methanol precipitation and analyzed using Western blots.

Antibodies

The following antibodies were used in this study: GFP, 1:100 (immunofluorescence [IF]; Merck Genei, Kenilworth, NJ), Ci, 1:10 (IF; Developmental Studies Hybridoma Bank [DSHB], Iowa City, IA), Hrs, 1:1000 (IF, Western blot [WB]; a kind gift from Hugo Bellen, Department of Molecular and Human Genetics, Baylor College of Medicine, Houston, TX), Okt9 (IF; 1:100) and GFP (1:500; WB; Santa Cruz Biotechnology, Dallas, TX), Col, 1:50 (IF; a kind gift from Michèle Crozatier and Alain Vincent, Centre de Biologie du Développement, Université de Toulouse, Toulouse, France), Alix, 1:500 (WB; a kind gift from Toshiro Aigaki, Department of Biological Sciences, Tokyo Metropolitan University, Tokyo, Japan), Vps28, 1:5000 (WB; a kind gift from Helmut Krämer, Department of Neuroscience and Department of Cell Biology, University of Texas Southwestern Medical Center, Dallas, TX), Shrub, 1:500 (WB; a kind gift from Fen-Biao Gao, Department of Neurology, University of Massachusetts Medical School, Worcester, MA); Hh, 1:100 or 1:500 (IF, WB; a kind gift from Suzanne Eaton, Max Planck Institute of Molecular Cell Biology and Genetics, Dresden, Germany), GM130, 1:200 (WB; Abcam, Cambridge, United Kingdom), Stx1a, 1:50 (WB; DSHB), Lbm, 1:50 (WB; DSHB), Csp, 1:50 (WB; DSHB), Ptc, 1:50 (IF; DSHB), β-galactosidase,1:25 (IF; DSHB), Rab7, 1:50 (IF; a kind gift from Akira Nakamura, Laboratory for Germline Development; RIKEN Center for Developmental Biology, Kobe, Hyogo, Japan), and cleaved caspase-3 (Asp-175), 1:500 (IF; Cell Signaling Technology, Danvers, MA). Anti-Hh antibody was also raised for this study (GenScript, Piscataway, NJ). Rabbits were immunized using

**$p < 0.01$. (D–I) *Drosophila* wing imaginal discs from WT (D, G) or expressing Shrub RNAi (E, H) or Vps4 RNAi (F, I) under the control of Hh-Gal4 and stained for Dpp-LacZ (D–F) or Ci (G–I) and imaged using FV1000 confocal microscope. Red lines indicate the extent of staining seen in each of the representative discs. Scale bar, 20 µm. (J) The traces (mean ± SD) indicate the distribution of Dpp-LacZ intensities along the A/P axis into the anterior obtained from the indicated number of wing imaginal discs for each treatment. A significant reduction in both intensities, as well as in spread, is seen in both Shrub and Vps4 RNAi conditions. (K) Box plot shows the median and the range of data obtained from the indicated number of discs of normalized length of the staining domain (average length of the stripe/length of the wing imaginal disc along the dorsoventral axis) of Ci under different conditions; ***$p < 0.001$.

a published sequence (Panáková *et al.*, 2005), and the peptide affinity-purified antibody was used for experiments. For immunofluorescence, secondary antibodies were obtained from Jackson ImmunoResearch Laboratories (Waltham, MA), and anti-mouse (1:100), anti-rabbit (1:100), anti-rat (1:150), and anti–guinea pig (1:100) were used. HRP-conjugated anti-mouse (1:5000), anti-rabbit (1:5000; Jackson ImmunoResearch Laboratories, West Grove, PA) and anti–guinea pig (1:5000; Thermo Scientific, Waltham, MA) were used for Western blots.

Immuno-EM

P100 and P250 were deposited on Formvar/carbon-coated EM grids and immunolabeled with anti-Hh (generated for this study: 1:20) and probed with a 5-nm protein A–gold conjugate (Cell Microscopy Centre Utrecht, Utrecht, Netherlands). Samples were postfixed using 1% glutaraldehyde and contrasted using a mixture of methyl cellulose and uranyl acetate (Beckett *et al.*, 2013). The grids were imaged on a Joel 1011 Transmission Electron Microscope at 80 kV or FEI Tecnai G2 Spirit. Cells and tissue samples were prepared for cryo-immune-EM according to the Tokuyasu method (Tokuyasu, 1980). Briefly, cells were fixed in 4% paraformaldehyde (PFA) plus 0.1% glutaraldehyde in PBS for 2 h at room temperature. Cells were then gently scraped and embedded in 10% gelatin. After an overnight infusion in poly(vinyl pyrrolidone)–sucrose, small blocks were mounted on aluminum pins and frozen in liquid nitrogen. Wing imaginal disc blocks in gelatin were processed similarly. Ultrathin sections (80–100 nm) were cut using a Leica UltracutUC6FCS microtome on a diamond knife (Diatome, Switzerland) and mounted on 100 hexagonal-mesh, Formvar/carbon-coated copper grids. Sections were stained using either anti-Hh (1:50) or anti-GFP (1:200; Clontech Laboratories, Mountain View, CA) and probed using a 10-nm protein A–gold conjugate (Cell Microscopy Centre Utrecht) or a gold-conjugated mouse secondary (British Biocell, Cardiff, United Kingdom).

Fluorescence correlation spectroscopy measurements

FCS measurements were made using the ConfoCor 2 module on a Zeiss 510 Meta confocal microscope. A 40×/1.2 numerical aperture water-immersion objective was used to focus the 488-nm laser line in the sample, and measurements were made from within the solution (100–200 µm from the coverslip). Each measurement is an averaged time trace over 10 iterations of 10 s each. The intensity data are autocorrelated using the onboard hardware correlator. The autocorrelation amplitude versus time data were fitted using the maximum entropy method (MEMFCS; Sengupta *et al.*, 2003) to obtain a distribution of time scales for all possible sizes. Based on the components extracted using this algorithm, the data were then analyzed using a model-dependent fit (two-component, three-dimensional [3D] diffusion) to obtain fractions of each component.

RNAi experiments

For double-strand RNA (dsRNA) treatment, ~5×10^5 HhGFP-transfected cells were plated in incomplete medium and treated with 7.5–10 of µg dsRNA. Four hours later, complete medium was added to the cells. On the fifth day, cell dsRNA was replenished. Cells were maintained in exosome production medium and assayed for secretion after 96 h of incubation. Subsequent processing of the samples was as in the vesicle isolation protocol mentioned earlier. Zeocin dsRNA was used as a control dsRNA (Gupta *et al.*, 2009). All of the dsRNA was commercially synthesized (Chromous Biotech, Bangalore, India). The source of the primers for some of the dsRNA was obtained from Open Biosystems (Huntsville, AL), and others were acquired from flyrnai.org. The primers used for the synthesis of dsRNA were as follows (F, forward; R, reverse):

Rab5 F: GAAGCAATATGCCGAGGAGA
Rab5 R: CAAATGAAATTCGTCCCCTG
Shrub F: ATGATCCAGACATGAAGCAGC
Shrub R: TCGATACAAAGCTAAGACTGCG
Vps4 F: AAAGGAGTACCTGAAGAAGGGC
Vps4 R: CAGATGGATCTTGAACATGACG
Vps28 F: GTCCATGATTGTGATGAACAGC
Vps28 R: TTTGAGCCAGAAACAAATTACG
Alix F: ACGTGGAGATCATGAAGTTGC
Alix R: ACGTGGAGATCATGAAGTTGC
Shibire F: TGAGCATCTGCTTCTGCAAC
Shibire R: AACCAAGCTGGATCTGATGG
Rab 27 F: GTCAGTAGCAGGGAGAACTCG
Rab27 R: ACCTGCAGATCTGGGACACC

Endocytic assays

Assays to detect the fate of endocytosed Hh were done by pulsing HhmCFP/HhK132DmCFP and LAMP-GFP dually transfected cells or HhmCFP/HhK132DmCFP singly transfected cells with A647-anti-GFP Fab; (1:100) for 20 min or 2 h, followed by wash using M1 buffer containing 2 mg/ml bovine serum albumin (BSA; Sigma-Aldrich) and 2 mg/ml glucose (M1BSAGlucose). Finally, the cells were fixed using 2.5% PFA for 20–30 min. For immunolabeling, cells were permeabilized using 0.37% NP-40 for 13 min. Blocking was done in M1BSAGlucose, and the cells were stained using primary (anti-Hrs) and secondary (anti–guinea pig) antibody for 1 h each. For endocytic assays, TMR-Dex was obtained from Life Technologies. Alexa dyes used for antibody conjugation, namely Alexa 568 (A568) and Alexa 647 (A647), were obtained from Life Technologies. Labeling kits to conjugate antibodies to these dyes were obtained from Amersham, and conjugation was carried out using the manufacturer's protocols.

Imaging was done using either the Olympus FV1000 confocal microscope or the Olympus microscope with PerkinElmer spinning disk as indicated.

To mark tubular lysosomes, HhmCFP/HhK132DmCFP–transfected cells were pulsed with labeled antibody along with TMR-Dex for 2 h and imaged live using the FV1000 confocal microscope in M1BSAGlucose.

For determining endocytic capacities of Hh variants, a surface accessibility assay was used. Transfected cells were labeled using as primary antibody A647–anti-GFP Fab (1:100) on ice for 30 min. One set of dishes was transferred to room temperature for 10 min and then transferred back on ice for binding of the secondary antibody (Alexa 568–labeled anti-mouse). Another set of dishes was bound by the secondary antibody without a shift to room temperature. Both sets of dishes were fixed using 2.5% PFA for 10 min on ice and then at room temperature for 20 min. Cells were imaged using the Olympus microscope with PerkinElmer spinning disk. The ratio of the intensities in the two channels was used to determine the surface accessibility of the secondary antibody to the primary antibody in a 10-min endocytic pulse.

For measuring fluid uptake in control and various other RNAi treatments, cells after 4 d of RNAi treatment were plated in coverslip bottom dishes. Cells were washed in M1BSAGlucose and pulsed with TMR-Dex (1 mg/ml) in SCM for 10 min, washed rigorously in M1BSAGlucose, and fixed for 25 min using 2.5% PFA. Imaging was carried out on a wide-field Nikon microscope.

Normalized TfR uptake in the case of Shibire RNAi was measured by a pulse of Alexa 568–conjugated transferrin (A568 transferrin) for 10 min. The bound A568 transferrin was then stripped from the cell surface using ascorbate buffer (pH 4) for 15 min. To mark the levels of TfR, cells were bound on ice with Alexa 647–conjugated anti-Okt9 antibody for 45 min. After washing in M1BSAGlucose, cells were fixed using 2.5% PFA for 10 min on ice followed by 20 min at room temperature. Imaging was carried out on a wide-field Nikon microscope.

Plasmids

The following plasmids were used for this study: UAS-HhGFP, UAS-HhmCFP UAS-HhK132DmCFP, UAS-HhΔCWmCFP (Vyas *et al.*, 2008), UAS-LAMP-GFP (Swetha *et al.*, 2011), UAS-GFP-GPI (Vyas *et al.*, 2008), Ptc-luciferase (a kind gift from Pascal Therond, Institut de Biologie de Valrose, Centre de Biochimie, Université Nice Sophia Antipolis, Nice, France), pMT-ss-HRP (a kind gift from Vivek Malhotra, Centre for Genomic Regulation, The Barcelona Institute of Science and Technology, Barcelona, Spain), and *Renilla* luciferase. UAS-HhK132DGFP and UAS-HhΔCWGFP were generated using standard cloning techniques (Chromous Biotech).

Fly stocks

The following fly stocks were used in this study: W^{1118} was used as a wild-type (WT) strain, and all flies were maintained at 25°C unless otherwise stated; Hh-Gal4, TubGal80ts (a kind gift from Xinhua Lin, State Key Laboratory of Biomembrane and Membrane Biotechnology, Institute of Zoology, Chinese Academy of Sciences, Beijing, China), Dpp-LacZ, TubGal80^{ts}; Hhgal4 (a kind gift from Pascal Therond), and Apterous-Gal4; TubGal80^{ts} (a kind gift from Douglas Allan, Department of Cellular and Physiological Sciences, University of British Columbia, Vancouver, BC, Canada). The UAS-ShrubRNAi (105887 KK) and UAS-Vps4RNAi (35125 GD) RNAi lines were obtained from the Vienna *Drosophila* RNAi Center (Vienna, Austria). UAS-Hid (head involution defective) was obtained from the Bloomington *Drosophila* Stock Center (Bloomington, IN).

Drosophila genetics

For RNAi experiments in the fly, animals carrying Hh-Gal4, TubGal80ts were crossed to Vps4 and Shrub RNAi lines driven by the UAS promoter. The crosses were maintained at 18°C. RNAi expression was induced by shifting the crosses at 29°C for 30 h for Shrub RNAi expression and 36 h in the case of Vps4 RNAi for Ptc, Dpp-LacZ, and caspase-3 staining. For Ci and Col staining, larvae were dissected 46 h after Vps4 RNAi expression. Apterous-Gal4; TubGal80ts was similarly crossed with the Shrub and Vps4 RNAi lines, and the resulting crosses were kept at 18°C. RNAi expression was induced by shifting the cross to 29°C for same time point as that with Hh-Gal4 for Shrub RNAi and 40 h for Vps4 RNAi expression. To induce apoptosis, the UAS-Hid line was crossed to Hh-Gal4, TubGal80ts, and the resulting crosses were maintained at 18°C followed by a shift at 29°C for 24 h before dissection.

Wing imaginal disc staining

Wing imaginal disc staining was carried out using standard procedures (Panáková *et al.*, 2005). Basically, wing imaginal discs were dissected out and fixed in 4% PFA for 20–30 min. These were then permeabilized in PBS containing 0.1% Triton X-100 (PBTx). Before staining, the discs were blocked in PBTx containing 4% BSA. Discs were stained using the primary antibodies overnight followed by washes using PBTx secondary antibodies for 2 h. Discs were washed after secondary antibody staining in PBTx and mounted in Vector shield mounting medium (Vector Laboratories, Burlingame, CA) and imaged using the Olympus FV1000 microscope. For extracellular staining, wing imaginal discs were fixed in 4% PFA for 20–30 min, blocked in PBS containing 4% BSA, and stained overnight using anti-Hh (1:15) antibody. Discs were washed in PBS and incubated with secondary antibody for 2 h. Mounting and imaging were done as described.

Luciferase reporter assay

Drosophila Clone8 cells were transfected using Ptc-luciferase reporter and the normalization vector (*Renilla* luciferase) in 30:1 ratio. P100 and P250 pellets (obtained by initial preconcentration of the medium using a 3-kDa filter) were added to the cells. Cells were lysed, and the luciferase activities were measured using the Dual-Luciferase Assay Kit (Promega, Madison, WI). The measurements were carried out after 40 h for the data shown in Figure 1 and 24 h for experiments involving Shrub RNAi.

Protease treatment of exovesicles

For identification of the topology of Hh on exosome-like vesicles, both P100 and P250 pellets resuspended in PBS were treated with or without proteinase K at a final concentration of 0.8 mg/ml in the presence or absence of 0.001% Triton X-100. Reaction was stopped after 30 min by addition of 5 mM phenylmethylsulfonyl fluoride. Samples were then analyzed using Western blots.

HRP secretion assay

Approximately 5×10^5 pMT-ss-HRP–transfected cells were plated in incomplete medium and treated with 7.5–10 µg of dsRNA. On the fifth day, medium was replaced by fresh SCM containing 0.5 mM copper sulfate. At 6 h later, cells were lysed, and HRP levels in the cell lysate and the medium (secreted) were measured using luminometry after addition of developing solution (Thermo Scientific).

Image analysis

Spread of Hh in the anterior domain. To measure the spread of Hh in discs, the grid function in image processing software MetaMorph was used. Intensities from a rectangular region (11×5 pixels) arranged in a linear array of 15 adjacent units were used to compute the intensity profile in a direction perpendicular to the A/P boundary. The average trace per disc was obtained from measurements from six adjacent linear arrays. The ratio of the intensities in the anterior/posterior was used to measure the extent of Hh spread in control and RNAi-treated conditions. The spread of extracellular Hh was also analyzed by taking intensity measurements from averaged confocal images by drawing region of interests using the MetaMorph tool in both posterior and the anterior regions of the wing imaginal disc.

Signaling readouts. Confocal images of wing imaginal discs were averaged to measure the length of the stripe of the signaling readout of Hh (Ci, Col Ptc). Line scans were taken from at least 10 regions across the entire stripe spanning the staining pattern, and the mean length was normalized to the length of the wing imaginal disc.

For Dpp-LacZ measurements, averaged confocal stacks were analyzed using the method described for Hh gradient measurements. Intensities from a rectangular region (11×5 pixels) arranged in adjacent linear array of 12 such units were used to compute the intensity

profile along the strip length. The average trace per disc was then obtained from measurements from six adjacent linear arrays.

Intensity and area measurements. For TfR uptake and normalized HhGFP levels at the surface, acquired images were subjected to local background subtraction, and intensities were measured from the background-subtracted images by drawing region of interests around the cells using tools available in MetaMorph. Area of endosomes was determined using the area function in MetaMorph. Endosomal area was calculated by setting a particular threshold and drawing region of interest around endosomes that were devoid of any signal from the surface.

Western blot quantification. Western blots were imaged using Image Quant LAS4000. After background subtraction, intensities were measured in the same manner as described for cells. For experiments involving RNAi treatment, the signal of HhGFP in the P100 and the P250 fractions for control and RNAi treatments was normalized to the signal of HhGFP in the cellular fraction of each condition. The normalized value thus obtained was compared across control and individual RNAi treatments. In the case of experiments involving Hh variants, signals in the P100 and P250 fractions were normalized with cellular signals of respective variants, and again the normalized value was used for comparison.

Statistics

An unpaired Student's *t* test was used in all experiments to determine the statistical significance of the data. A one-sample *t* test was used for quantifications involving Western blots.

ACKNOWLEDGMENTS

We thank Hugo Bellen, Toshiro Aigaki, Suzanne Eaton, Fen-Biao Gao, Helmut Kramer, Michèle Crozatier, Alain Vincent, Akira Nakamura, Pascal Therond, Donald Ready, Xinhua Lin, and Douglas Allan for sharing reagents. R.G.P. was supported by grants from the National Health and Medical Research Council of Australia (1037320 and 1045092). We acknowledge the facilities and scientific and technical assistance from staff of the Australian Microscopy and Microanalysis Facility at the Centre for Microscopy and Microanalysis, University of Queensland. We thank H. Krishnamurthy and M. Mathew of the Central Imaging and Flow Cytometry Facility (National Centre for Biological Sciences) and Renu Pasricha and K. M. Yatheendran at the TEM Facility for their support. We acknowledge the National Centre for Biological Sciences and Centre of Excellence project BT/01/COE/09/01 funded by the Department of Biotechnology (India) for research support and a graduate fellowship (A.P.), the Wellcome Trust/DBT India Alliance for an Early Career Fellowship (N.V.), and a J. C. Bose Fellowship, Department of Science and Technology, Government of India (S.M.).

REFERENCES

Aikin R, Cervantes A, D'Angelo G, Ruel L, Lacas-Gervais S, Schaub S, Thérond P (2012). A genome-wide RNAi screen identifies regulators of cholesterol-modified hedgehog secretion in Drosophila. PLoS One 7, e33665.

Ayers KL, Gallet A, Staccini-Lavenant L, Thérond PP (2010). The long-range activity of Hedgehog is regulated in the apical extracellular space by the glypican Dally and the hydrolase Notum. Dev Cell 18, 605–620.

Bard F, Casano L, Mallabiabarrena A, Wallace E, Saito K, Kitayama H, Guizzunti G, Hu Y, Wendler F, Dasgupta R, *et al*. (2006). Functional genomics reveals genes involved in protein secretion and Golgi organization. Nature 439, 604–607.

Beckett K, Monier S, Palmer L, Alexandre C, Green H, Bonneil E, Raposo G, Thibault P, Le Borgne R, Vincent J-P (2013). Drosophila S2 cells secrete wingless on exosome-like vesicles but the wingless gradient forms independently of exosomes. Traffic 14, 82–96.

Bilioni A, Sánchez-Hernández D, Callejo A, Gradilla A-C, Ibáñez C, Mollica E, Carmen Rodríguez-Navas M, Simon E, Guerrero I (2013). Balancing Hedgehog, a retention and release equilibrium given by Dally, Ihog, Boi and shifted/DmWif. Dev Biol 376, 198–212.

Bischoff M, Gradilla A-C, Seijo I, Andrés G, Rodríguez-Navas C, González-Méndez L, Guerrero I (2013). Cytonemes are required for the establishment of a normal Hedgehog morphogen gradient in Drosophila epithelia. Nat Cell Biol 15, 1269–1281.

Briscoe J, Thérond PP (2013). The mechanisms of Hedgehog signalling and its roles in development and disease. Nat Rev Mol Cell Biol 14, 416–429.

Bucci C, Parton RG, Mather IH, Stunnenberg H, Simons K, Hoflack B, Zerial M (1992). The small GTPase rab5 functions as a regulatory factor in the early endocytic pathway. Cell 70, 715–728.

Burke R, Nellen D, Bellotto M, Hafen E, Senti KA, Dickson BJ, Basler K (1999). Dispatched, a novel sterol-sensing domain protein dedicated to the release of cholesterol-modified hedgehog from signaling cells. Cell 99, 803–815.

Callejo A, Bilioni A, Mollica E, Gorfinkiel N, Andrés G, Ibáñez C, Torroja C, Doglio L, Sierra J, Guerrero I (2011). Dispatched mediates Hedgehog basolateral release to form the long-range morphogenetic gradient in the Drosophila wing disk epithelium. Proc Natl Acad Sci USA 108, 12591–12598.

Chan CC, Scoggin S, Wang D, Cherry S, Dembo T, Greenberg B, Jin EJ, Kuey C, Lopez A, Mehta SQ, *et al*. (2011). Systematic discovery of Rab GTPases with synaptic functions in Drosophila. Curr Biol 21, 1704–1715.

Chiang C, Litingtung Y, Lee E, Young KE, Corden JL, Westphal H, Beachy PA (1996). Cyclopia and defective axial patterning in mice lacking Sonic hedgehog gene function. Nature 383, 407–413.

D'Angelo G, Matusek T, Pizette S, Thérond PP (2015). Endocytosis of Hedgehog through Dispatched regulates long-range signaling. Dev Cell 290–303.

Dessaud E, McMahon AP, Briscoe J (2008). Pattern formation in the vertebrate neural tube: a sonic hedgehog morphogen-regulated transcriptional network. Development 135, 2489–2503.

Fader CM, Colombo MI (2009). Autophagy and multivesicular bodies: two closely related partners. Cell Death Differ 16, 70–78.

Gradilla AC, González E, Seijo I, Andrés G, Bischoff M, González-Mendez L, Sánchez V, Callejo A, Ibáñez C, Guerra M, *et al*. (2014). Exosomes as Hedgehog carriers in cytoneme-mediated transport and secretion. Nat Commun 5, 5649.

Gross JC, Chaudhary V, Bartscherer K, Boutros M (2012). Active Wnt proteins are secreted on exosomes. Nat Cell Biol 14, 1036–1045.

Guha A, Sriram V, Krishnan KS, Mayor S (2003). Shibire mutations reveal distinct dynamin-independent and -dependent endocytic pathways in primary cultures of Drosophila hemocytes. J Cell Sci 116, 3373–3386.

Gupta GD, Swetha MG, Kumari S, Lakshminarayan R, Dey G, Mayor S (2009). Analysis of endocytic pathways in Drosophila cells reveals a conserved role for GBF1 in internalization via GEECs. PLoS One 4, e6768.

Henne WM, Stenmark H, Emr SD (2013). Molecular mechanisms of the membrane sculpting ESCRT pathway. Cold Spring Harb Perspect Biol 5, a016766.

Hsu C, Morohashi Y, Yoshimura S, Manrique-Hoyos N, Jung S, Lauterbach MA, Bakhti M, Grønborg M, Möbius W, Rhee J, *et al*. (2010). Regulation of exosome secretion by Rab35 and its GTPase-activating proteins TBC1D10A-C. J Cell Biol 189, 223–232.

Johannes L, Mayor S (2010). Induced domain formation in endocytic invagination, lipid sorting, and scission. Cell 142, 507–510.

Katanaev VL, Solis GP, Hausmann G, Buestorf S, Katanayeva N, Schrock Y, Stuermer CA, Basler K (2008). Reggie-1/flotillin-2 promotes secretion of the long-range signalling forms of Wingless and Hedgehog in Drosophila. EMBO J 27, 509–521.

Khare N, Baumgartner S (2000). Dally-like protein, a new Drosophila glypican with expression overlapping with wingless. Mech Dev 99, 199–202.

Koles K, Nunnari J, Korkut C, Barria R, Brewer C, Li Y, Leszyk J, Zhang B, Budnik V (2012). Mechanism of evenness interrupted (Evi)-exosome release at synaptic boutons. J Biol Chem 287, 16820–16834.

Lawrence SP, Bright NA, Luzio JP, Bowers K (2010). The sodium/proton exchanger NHE8 regulates late endosomal morphology and function. Mol Biol Cell 21, 3540–3551.

Li J, Liu K, Liu Y, Xu Y, Zhang F, Yang H, Liu J, Pan T, Chen J, Wu M, *et al*. (2013). Exosomes mediate the cell-to-cell transmission of IFN-α-induced antiviral activity. Nat Immunol 14, 793–803.

Liégeois S, Benedetto A, Garnier J-M, Schwab Y, Labouesse M (2006). The V0-ATPase mediates apical secretion of exosomes containing Hedgehog-related proteins in Caenorhabditis elegans. J Cell Biol 173, 949–961.
Matsuo H, Chevallier J, Mayran N, Le Blanc I, Ferguson C, Fauré J, Blanc NS, Matile S, Dubochet J, Sadoul R, *et al*. (2004). Role of LBPA and Alix in multivesicular liposome formation and endosome organization. Science 303, 531–534.
Matusek T, Wendler F, Polès S, Pizette S, D'Angelo G, Fürthauer M, Thérond PP (2014). The ESCRT machinery regulates the secretion and long-range activity of Hedgehog. Nature 516, 99–103.
Meckes DG, Raab-Traub N (2011). Microvesicles and viral infection. J Virol 85, 12844–12854.
Meiser A, Sancho C, Krijnse Locker J (2003). Plasma membrane budding as an alternative release mechanism of the extracellular enveloped form of vaccinia virus from HeLa cells. J Virol 77, 9931–9942.
Méthot N, Basler K (1999). Hedgehog controls limb development by regulating the activities of distinct transcriptional activator and repressor forms of Cubitus interruptus. Cell 96, 819–831.
Michel M, Kupinski AP, Raabe I, Bökel C (2012). Hh signalling is essential for somatic stem cell maintenance in the Drosophila testis niche. Development 139, 2663–2669.
Nakamura N, Rabouille C, Watson R, Nilsson T, Hui N, Slusarewicz P, Kreis TE, Warren G (1995). Characterization of a cis-Golgi matrix protein, GM130. J Cell Biol 131, 1715–1726.
Nozawa YI, Lin C, Chuang P-T (2013). Hedgehog signaling from the primary cilium to the nucleus: an emerging picture of ciliary localization, trafficking and transduction. Curr Opin Genet Dev 23, 429–437.
Nüsslein-Volhard C, Wieschaus E (1980). Mutations affecting segment number and polarity in Drosophila. Nature 287, 795–801.
Ostrowski M, Carmo NB, Krumeich S, Fanget I, Raposo G, Savina A, Moita CF, Schauer K, Hume AN, Freitas RP, *et al*. (2010). Rab27a and Rab27b control different steps of the exosome secretion pathway. Nat Cell Biol 12, 19–30; supplement, 1–13.
Panáková D, Sprong H, Marois E, Thiele C, Eaton S (2005). Lipoprotein particles are required for Hedgehog and Wingless signalling. Nature 435, 58–65.
Pepinsky RB, Zeng C, Wen D, Rayhorn P, Baker DP, Williams KP, Bixler SA, Ambrose CM, Garber EA, Miatkowski K, *et al*. (1998). Identification of a palmitic acid-modified form of human Sonic hedgehog. J Biol Chem 273, 14037–14045.
Peters C, Wolf A, Wagner M, Kuhlmann J, Waldmann H (2004). The cholesterol membrane anchor of the Hedgehog protein confers stable membrane association to lipid-modified proteins. Proc Natl Acad Sci USA 101, 8531–8536.
Porter JA, von Kessler DP, Ekker SC, Young KE, Lee JJ, Moses K, Beachy PA (1995). The product of hedgehog autoproteolytic cleavage active in local and long-range signalling. Nature 374, 363–366.
Sengupta P, Garai K, Balaji J, Periasamy N, Maiti S (2003). Measuring size distribution in highly heterogeneous systems with fluorescence correlation spectroscopy. Biophys J 84, 1977–1984.
Sriram V, Krishnan KS, Mayor S (2003). deep-orange and carnation define distinct stages in late endosomal biogenesis in Drosophila melanogaster. J Cell Biol 161, 593–607.
Stoeck A, Keller S, Riedle S, Sanderson MP, Runz S, Le Naour F, Gutwein P, Ludwig A, Rubinstein E, Altevogt P (2006). A role for exosomes in the constitutive and stimulus-induced ectodomain cleavage of L1 and CD44. Biochem J 393, 609–618.
Swetha MG, Sriram V, Krishnan KS, Oorschot VMJ, ten Brink C, Klumperman J, Mayor S (2011). Lysosomal membrane protein composition, acidic pH and sterol content are regulated via a light-dependent pathway in metazoan cells. Traffic 12, 1037–1055.
Tabata T, Takei Y (2004). Morphogens, their identification and regulation. Development 131, 703–712.
Tokuyasu KT (1980). Immunochemistry on ultrathin frozen sections. Histochem J 12, 381–403.
Torroja C, Gorfinkiel N, Guerrero I (2005). Mechanisms of Hedgehog gradient formation and interpretation. J Neurobiol 64, 334–356.
Trajkovic K, Hsu C, Chiantia S, Rajendran L, Wenzel D, Wieland F, Schwille P, Brügger B, Simons M (2008). Ceramide triggers budding of exosome vesicles into multivesicular endosomes. Science 319, 1244–1247.
Tukachinsky H, Kuzmickas RP, Jao CY, Liu J, Salic A (2012). Dispatched and scube mediate the efficient secretion of the cholesterol-modified hedgehog ligand. Cell Rep 2, 308–320.
Vaccari T, Rusten TE, Menut L, Nezis IP, Brech A, Stenmark H, Bilder D (2009). Comparative analysis of ESCRT-I, ESCRT-II and ESCRT-III function in Drosophila by efficient isolation of ESCRT mutants. J Cell Sci 122, 2413–2423.
Vyas N, Goswami D, Manonmani A, Sharma P, Ranganath HA, VijayRaghavan K, Shashidhara LS, Sowdhamini R, Mayor S (2008). Nanoscale organization of hedgehog is essential for long-range signaling. Cell 133, 1214–1227.
Vyas N, Walvekar A, Tate D, Lakshmanan V, Bansal D, Lo Cicero A, Raposo G, Palakodeti D, Dhawan J (2014). Vertebrate Hedgehog is secreted on two types of extracellular vesicles with different signaling properties. Sci Rep 4, 7357.
Yan D, Wu Y, Yang Y, Belenkaya TY, Tang X, Lin X (2010). The cell-surface proteins Dally-like and Ihog differentially regulate Hedgehog signaling strength and range during development. Development 137, 2033–2044.